MAX-PLANCK-INSTITUT FÜR PLASMAPHYSIK

GARCHING BEI MÜNCHEN

Cyclotron Radiation from Toroidal Plasmas

F. Pohl

IPP
6/161 July 1977

Die nachstehende Arbeit wurde im Rahmen des Vertrages zwischen dem Max-Planck-Institut für Plasmaphysik und der Europäischen Atomgemeinschaft über die Zusammenarbeit auf dem Gebiete der Plasmaphysik durchgeführt.

IPP 6/161

F. Pohl

Cyclotron Radiation from Toroidal Plasmas

Abstract

In this report cyclotron emission of a toroidal or cylindrical plasma is calculated on the assumption of MAXWELL-distributed electrons and KIRCHHOFF's law. The plasma density and temperature depend only on the distance r from the minor torus axis, wall reflectivity being taken into account.

The radiation intensity at the plasma surface is computed numerically; some formulae interpolating the results are given.

Furthermore, some spectra are presented in which the specific intensity is plotted versus the frequency.

Table of Contents

§1 Introduction

Cyclotron radiation is caused by plasma electrons gyrating in a magnetic field. The contribution made by ions to cyclotron radiation is negligible.

The cyclotron emission of a plasma volume element depends on the electron density, electron temperature, magnetic field, etc., and so it is possible by measuring the cyclotron radiation to determine, for example, the electron temperature (see, for example, CANO /1/). It is only the radiation which reaches the plasma surface that can be measured. This paper is therefore concerned with the radiation intensity $\frac{\partial^2 E}{\partial S \partial t}$, i.e. the energy ($\partial^2 E$) emerging in the time-interval (∂t) through area (∂S) from the plasma surface, and with the differential intensity or spectral function, i.e. the intensity per unit frequency-interval per unit solid angle, or the contribution of a given direction and frequency to the total intensity. The paper is set out as follows:

In §2 we explain the terms used, such as light path, test point, etc., and present the formulae which are independent of the geometry (torus, slab etc.) and of the symmetry properties of the plasma parameters. These are the integral formula for the intensity, spectral function, optical depth, and the absorption coefficient. It will be seen that it is easy to write an integral formula for the intensity, but that it cannot be put to use until a series of assumptions is introduced:

1. KIRCHHOFF's law.
2. Refractive index of the plasma = 1.
3. Maxwell distribution of the electrons.

   In §3 and §4 we also assume:

4. Toroidal geometry.
5. Magnetic field inversely proportional to the distance from the major torus axis.
6. Density and temperature depend only on the distance r from the minor torus axis.

At the usual laboratory plasma temperatures of a few keV the absorption coefficient as a function of the radiation frequency has sharp maxima when the radiation frequency is (approximately) an integral multiple of the gyration frequency. Therefore, at not too high frequencies cyclotron radiation is emitted or absorbed just at certain locations in the plasma, the "resonance points". In §5 we therefore use a δ-function ansatz for the absorption coefficient. When a resonance point is opaque, the spectral function is proportional to the electron temperature at that point (see eq. (5.7a)). The position of the resonance points depends on frequency; if the above mentioned conditions are satisfied, it is therefore possible to determine the temperature profile from an experimental cyclotron radiation spectrum.

Unfortunately, the thermal emission treated in this paper is often dominated by non-thermal emission (run-aways; see ref./6/,/7/), which may exceed the thermal emission by orders of magnitude, as can be estimated from our formula in §8.

§2 Intensity and spectral function

To describe the cyclotron emission from the plasma, we use the concepts intensity, spectral function, test point and light path. The test point is the point at which the intensity and spectral function are to be determined. Let us imagine a microwave receiver (horn) mounted at this point and aligned in a certain direction, i.e. it only records radiation coming from the direction ϑ, ψ. The path which this radiation has traversed in the plasma we call the "light path" (see ENGELMANN /2/).

We define ϑ as the angle between the tangent located in the equatorial plane of the torus (in §3 this is the y direction) and the light path (see Fig. 1); (2.1)

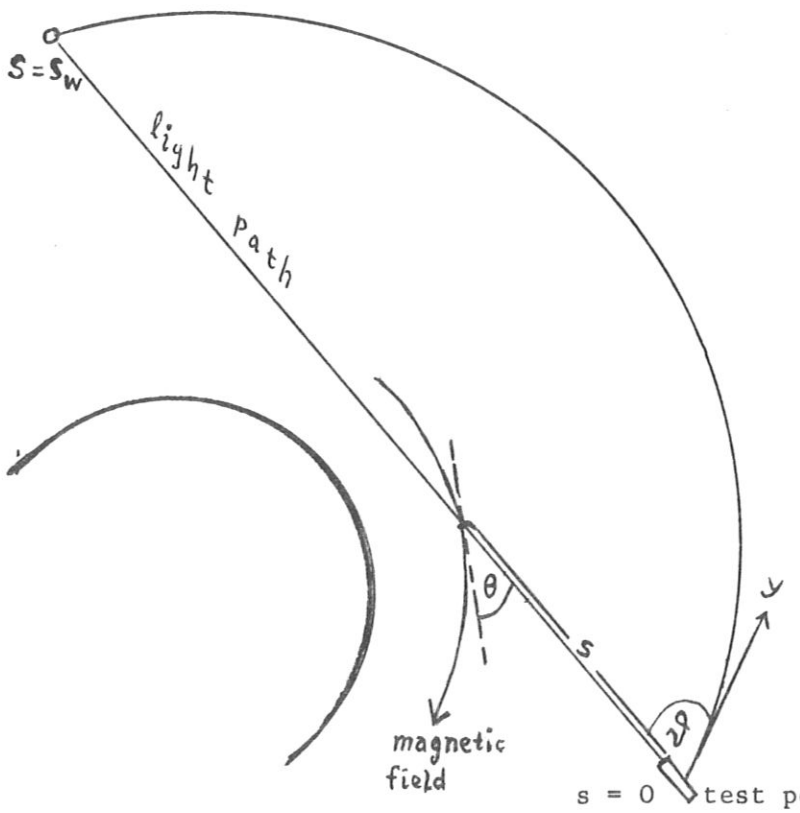

Fig. 1
Definition of ϑ and $\theta(s)$

/2/ F. ENGELMANN, M. CURATOLO
Nucl. Fusion 13 (1973), p. 497

s is the distance from the test pont, measured along the light path; (2.2)

$\Theta(s)$ is the angle between the magnetic field and light path; (2.3)

ψ is the angle between the surface normal and the projection of the light path (see Fig. 5, §3). (2.4)

We now derive the integral formulae for the intensity and spectral function. The surface element dS, when observed from the volume element dV located at s, forms solid angle

$$d\tilde{\Omega} = \frac{\sin\vartheta \cos\psi}{s^2} \, dS \, . \tag{2.5}$$

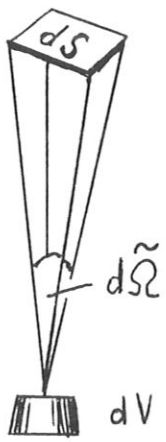

Fig. 2a

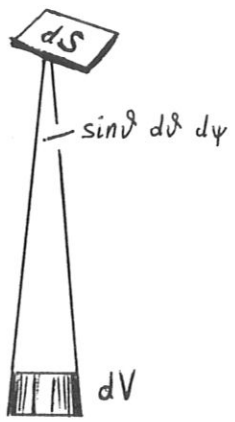

Fig. 2b

The radiation pencil

We choose the volume elements dV so that from the test point they form at the same solid angle $\sin\vartheta \, d\vartheta \, d\psi$,

i.e. $dV = s^2 \, ds \, \sin\vartheta \, d\vartheta \, d\psi$ (2.6)

The dV thus occupy a pencil-like volume which CHANDRSEKHAR calls the radiation pencil. The emission from dV to dS is $\eta(s) \, dV \, d\tilde{\Omega} \, d\omega$.

Of this only the fraction $e^{-\tau(s)}$ arrives at dS .

It follows that

$$\frac{\partial^2 E}{\partial \zeta \partial t} = \int_0^{\pi} d\vartheta \sin^2\vartheta \int_{-\pi/2}^{+\pi/2} d\psi \cos\psi \int_0^{\infty} d\omega \int_0^{s_w} e^{-\tau(s)} \eta(s)\, ds \tag{2.7}$$

with $$\tau(s) = \int_0^s \alpha(\tilde{s})\, d\tilde{s} \tag{2.8}$$

$\tau(s)$ = optical thickness of the plasma between o and s,

α = reciprocal energy absorption length,

s_w = light path length

Equation (2,5) and the integration limits given in eq. (2.7) are always valid when the axis on which ϑ is aligned (in §3 the y axis) is perpendicular to the surface normal. Equation (2.7) is valid for <u>any</u> geometry.

In real plasmas light is refracted, thus making the light path curved. As announced in the introduction, we now make the following assumptions in eq. (2.7):

1. The light path is straight,

   i.e. the refractive index of the plasma is 1, (2.9)

   i.e. the dielectric constant of the plasma is 1. (2.10)

   Of course, this assumption imposes a constraint on the domain of validity: the representation shown here <u>may</u> be wrong for

$$\omega \lesssim 2\omega_p \tag{2.11}$$

   and in an interval of width

$$\Delta\omega \gtrsim \frac{\omega_p^2}{n\omega_H} \tag{2.12}$$

in the vicinity of the resonance points $\omega \approx n\omega_H$. (2.13)

2. The electrons are in equilibrium so that KIRCHHOFF's law is applicable:

$$\eta = \frac{\alpha\, kT_e \omega^2}{8\,\pi^3\, c^2}$$

If T_e is measured in keV, one obtains $kT_e/m_e c^2 = T_e/511$ (2.14a)

and hence

$$\eta = 7.89 \times 10^{-6}\, m_e T_e \omega^2 \alpha \qquad (2.14)$$

Substituting eq. (2.14) in eq. (2.7) yields

$$\frac{\partial^2 E}{\partial S \partial t} = m_e \omega_T^3\, I \qquad (2.15)$$

with

$$I = 7.89 \times 10^{-6} \int_0^{\pi} d\vartheta \sin^2\vartheta \int_{-\pi/2}^{\pi/2} d\psi \cos\psi \int_0^{\infty} d\Omega_T\, Y \qquad (2.16)$$

where the spectral function

$$Y = \Omega_T^2 \int_0^{s_w} ds\, e^{-\tau(s)}\, \alpha(s)\, T_e(s)\, ds \qquad (2.17)$$

$$\Omega_T = \omega/\omega_T \qquad (2.18)$$

ω_T = cyclotron frequency at an arbitrarily chosen location (see eq. (5.5)).

KIRCHHOFF's law contains the assumption that the electrons have a temperature

T_e and therefore have a MAXWELL distribution. From this it follows that

$$\alpha(s) = \frac{\omega_p^2(s)}{c\omega_H(s)} \; A\left(\Theta(s); \frac{\omega}{\omega_H(s)}; \frac{511}{T_e(s)}\right) \tag{2.19}$$

where A is the dimensionless absorption coefficient, depending only on three dimensionless variables (see §10).

§3 Torus geometry

In this section we introduce a Cartesian coordinate system whose z axis coincides with the major torus axis. We determine the coordinates of the test point (eq. (3.1)) and the direction cosine of the light path (eq. (3.2)) and can then find Cartesian coordinates for every s (eq. (3.3)). Owing to the symmetry properties of the plasma we also require the torus coordinates (eq. 3.4) in addition to the Cartesian coordinates. For we shall later assume (eq. (4.2)) that, for example, the electron temperature T_e only depends on the distance r (eq. 3.4b)) from the minor torus axis. Therefore, to determine the function $T_e(s)$ occuring in eq. (2.17), one first has to calculate the value of r for the given s (eq. (3.4b)). Furthermore, from the toroidal and poloidal magnetic field components we calculate the corresponding Cartesian components of the magnetic field $\vec{H}$ (eq. (3.5)) and from these the angle Θ(eq. (3.6)), which is required in eq. (2.19) as a function of s.

Test point

The torus has a major radius R_G and minor radius R_K.

The test point is described in terms of the angle ϕ_A.

The test point is assumed to be located in the x-z plane. It then follows that

$$x_A = R_G - R_K \cos \phi_A \quad , \tag{3.1a}$$

$$y_A = 0 \quad , \tag{3.1b}$$

$$z_A = R_K \sin \phi_A \quad . \tag{3.1c}$$

Fig. 3 shows
the x-z plane with
test point;
z axis = major torus axis
x-y plane = equatorial plane

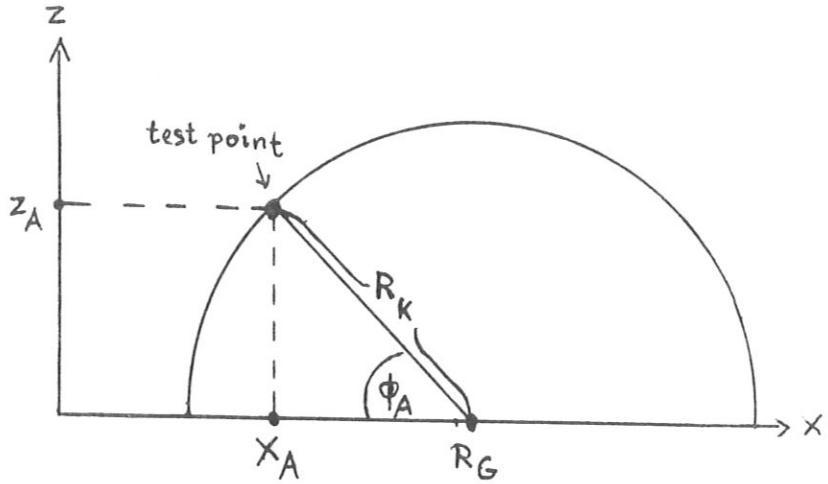

Light path

Fig. 4 shows
the light path with a torus
segment in spatial perspective.

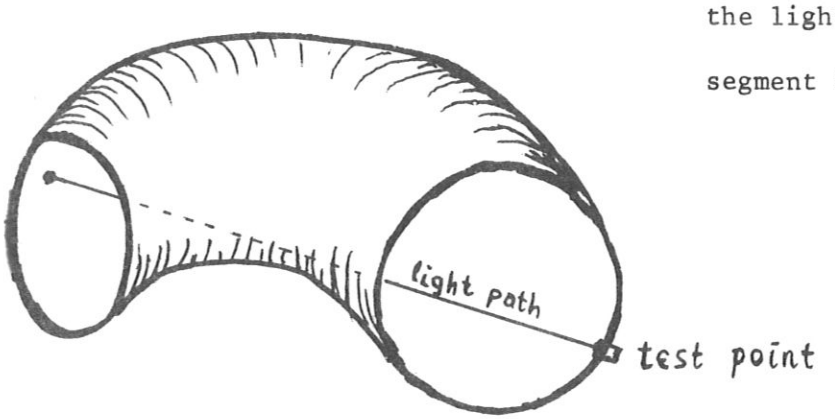

Fig. 5 shows
the projection of Fig. 4
onto the x-z plane.

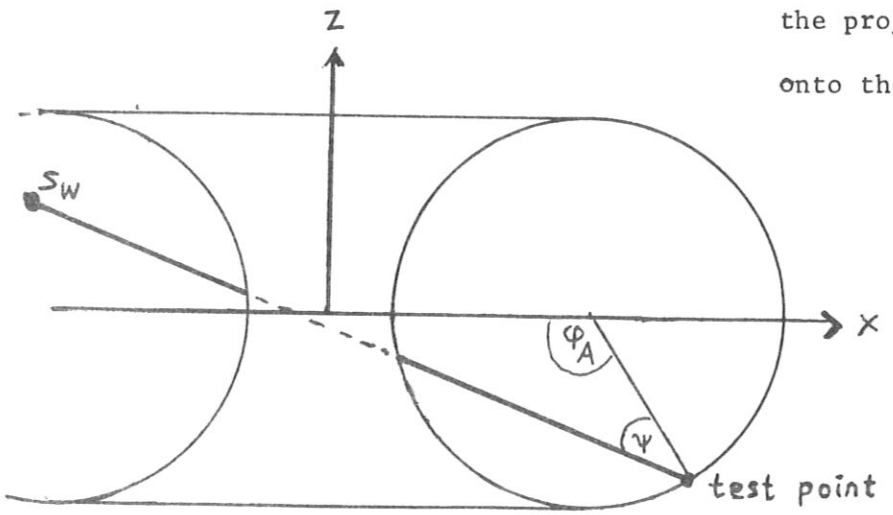

The magnetic field at the test point is in the y direction (if the plasma current vanishes). The unit vector in the direction of the light path has the Cartesian coordinates

$$e_x = \sin\vartheta \cos(\psi-\phi_A) \quad , \tag{3.2a}$$

$$e_y = \cos\vartheta \quad , \tag{3.2b}$$

$$e_z = \sin\vartheta \sin(\psi-\phi_A) \quad . \tag{3.2c}$$

From eq. (3.2) it follows that the Cartesian coordinates of the point located at the distance s from the test point are

$$x = x_A + e_x s \quad , \tag{3.3a}$$

$$y = y_A + e_y s \quad , \tag{3.3b}$$

$$z = z_A + e_z s \quad . \tag{3.3c}$$

Torus coordinates

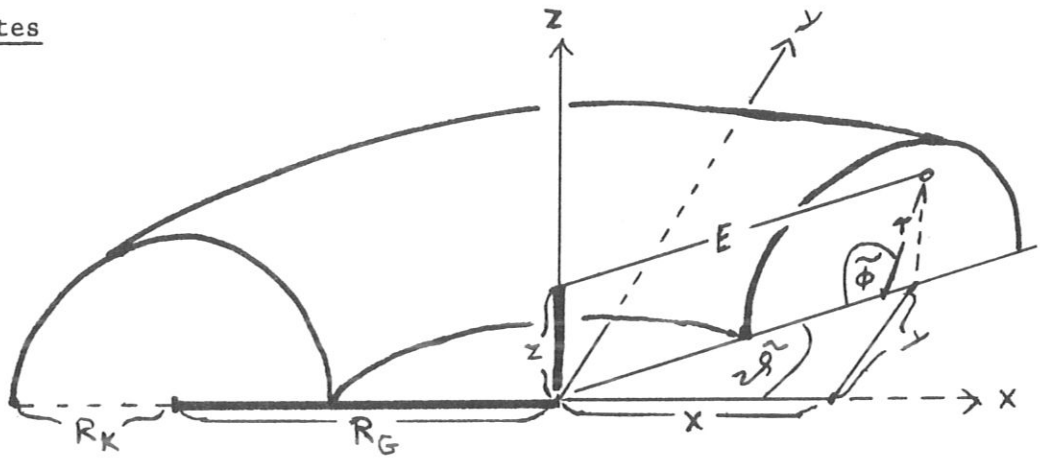

Fig. 6 shows a torus with major radius R_G and minor radius R_K, and a point with the Cartesian coordinates x, y, z and the torus coordinates r, $\tilde{\phi}$, $\tilde{\vartheta}$.

From Fig. 6 it follows that

$$E = \sqrt{x^2 + y^2} \quad , \tag{3.4a}$$

$$r = \sqrt{(R_G - E)^2 + Z^2} \quad , \tag{3.4b}$$

$$\sin \tilde{\vartheta} = y/E \quad , \tag{3.4c}$$

$$\cos \tilde{\vartheta} = x/E \quad , \tag{3.4d}$$

$$\sin \tilde{\phi} = z/r \quad , \tag{3.4e}$$

$$\cos \tilde{\phi} = (R_G - E)/r \quad . \tag{3.4f}$$

Magnetic field

It is assumed that the magnetic field has a toroidal component H_{tor} and a poloidal component H_{pol}, but no component in the r direction. It then follows from the geometry (Figs. 7 and 8) that the Cartesian magnetic field components are

$$H_x = H_{pol}\sin\tilde{\phi}\cos\tilde{\vartheta} - H_{tor}\sin\tilde{\vartheta} \quad (3.5a)$$

$$H_y = H_{pol}\sin\tilde{\phi}\sin\tilde{\vartheta} + H_{tor}\cos\tilde{\vartheta} \quad (3.5b)$$

$$H_z = H_{pol}\cos\tilde{\phi} \quad (3.5c)$$

$$H = \sqrt{H_{pol}^2 + H_{tor}^2} \quad (3.5d)$$

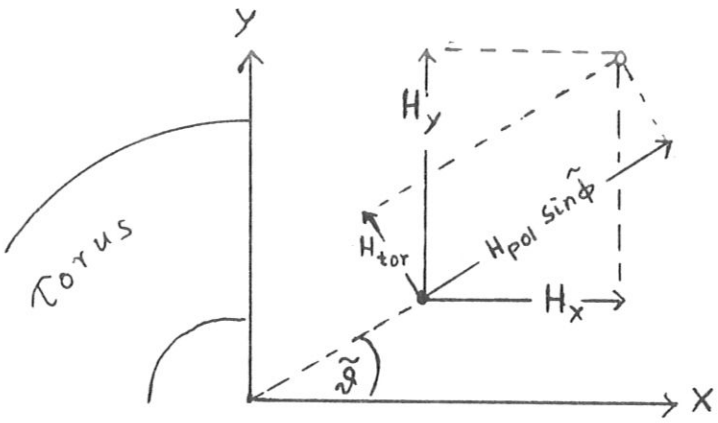

Fig. 7
The components in the equatorial plane

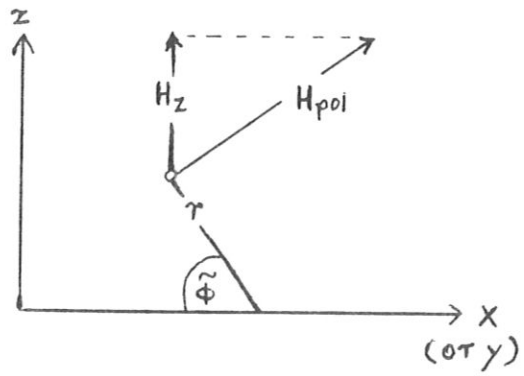

Fig. 8
The components in the x - z - plane (or y - z - plane)

For the angle Θ between the magnetic field and the light path one has

$\cos\Theta$ = scalar product of the unit vectors in the directions of the magnetic field and light path

$$\cos\Theta = \frac{1}{H}\,(H_x e_x + H_y e_y + H_z e_z) \tag{3.6}$$

Light path length s_w

If eq.(3.3) is substituted in eq.(3.4), every s is thereby assigned a value r(s). s_w is the smallest $s > 0$ for which

$$r(s) = R_K \tag{3.7}$$

is valid; for at the location where the light path passes through the torus surface one has $r = R_K$.

Equation (3.7) is a biquadratic equation in s; it is later solved numerically by interval nesting.

In the special case

$\vartheta = 90^\circ$

$\psi = 0$

it follows that

$$s_w = 2R_K. \tag{3.7a}$$

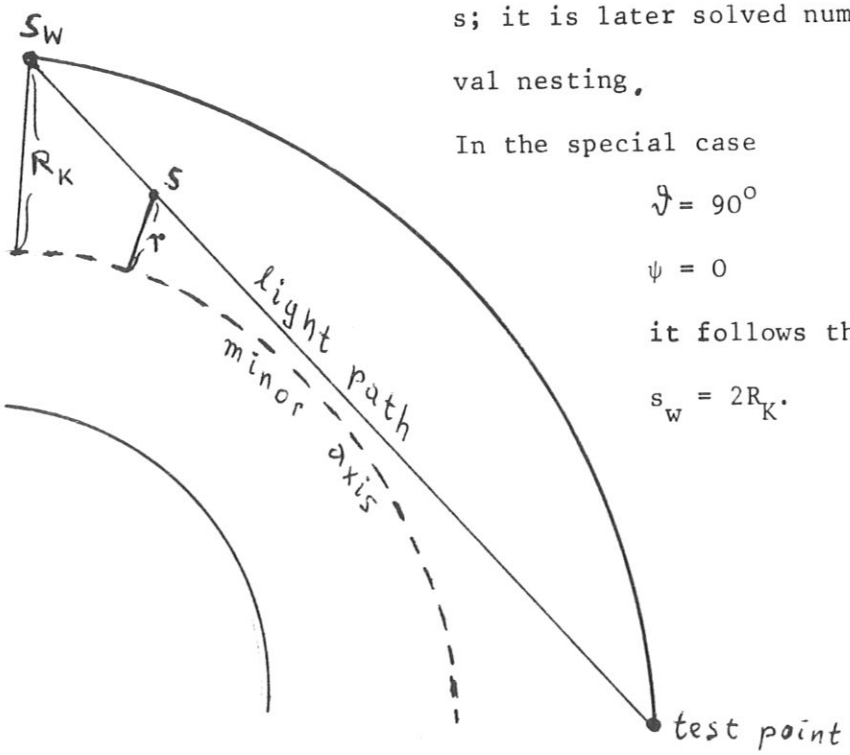

§4 Plasma parameters

It is assumed here that:

1. The density and temperature depend only on the distance r from the minor torus axis:

$$n_e = D_M(1-\hat{r}^2)^{p_D} \quad , \tag{4.1}$$

$$T_e = T_M(1-\hat{r}^2)^{p_T} \quad , \tag{4.2}$$

$$\hat{r} = r/R_K \leq 1 \quad , \tag{4.3}$$

where

D_M = density in the centre = minor torus axis, (4.4)

T_M = temperature in the centre,

p_D = density profile number,

p_T = temperature profile number,

p_D = 0 denotes box profile,

p_D = 1 denotes parabolic profile,

p_D = 2 denotes bell-shaped profile.

2. The toroidal component of the magnetic field is

$$H_{tor} = H_T \cdot R_G/E \quad , \tag{4.11}$$

where E is the distance from the major axis (see eq. (3.4a)).

The plasma current I_p generates a poloidal magnetic field of the order

$$H_{pol} = \frac{I_p}{5R_K}\,\hat{r}\,(2-\hat{r}^2) \quad , \tag{4.12}$$

where H is to be given in gauss, I_p in ampere, and R_K in cm.

Equation (4.12) is exactly valid for parabolic current density

$$j \text{ prop. } 1-\hat{r}^2 \tag{4.13}$$

and

$$\text{aspect ratio } R_K/R_G \to 0 \text{ (cylindrical plasma).} \tag{4.14}$$

Particularly in the case of fat tori there may be large deviations from eq. (4.12); fortunately, one has $H_{pol} << H_{tor}$. The cyclotron emission depends on the following parameters:

$$D_M;\ H_T;\ I_p;\ p_T;\ R_{EFL};\ R_G;\ R_K;\ T_M;\ \phi_A\ ;\ \mathcal{P} \tag{4.15}$$

These parameters have to be read into a program for numerical calculations; R_{EFL} describes the reflectivity of the wall (see §7). The spectral function Y also depends on

$$\Theta;\ \psi;\ \Omega_T\ . \tag{4.16}$$

Owing to the symmetry properties the parameters

$$D_M;\ H_T;\ R_G;\ R_K$$

occur only in the combinations

$$A_{SPEKT} = R_G \,/\, R_K \tag{4.17}$$

$$D = \omega_M^2\, R_K \,/\, (c\ \omega_T) \quad = \underline{\text{dimensionless minor radius.}} \tag{4.18}$$

If $I_P = 0$

it follows that

$$D = 60.36\ \frac{D_M[10^{13}\,cm^{-3}]\ R_K\,[cm]}{H_T\,[kG]}\ .$$

§5 Spectral function in δ approximation

In the case of fat tori the cyclotron emission of a light path is often generated at only one or two resonance points whose width Δs is small relative to the length of the light path. In such cases it holds that

$$\alpha(s) = \sum_m \tau_m \ \delta\ (s-s_m) \tag{5.1}$$

where s_1 = resonance point nearest to the test point (see Fig. 9),

$$\tau_m = \int_{(s_m)} \alpha\ (s)ds = \text{optical depth of the resonance at } s_m, \tag{5.2}$$

(s_m) = vicinity of s_m.

Note: $\tau(s) = \int_0^s \alpha\ (\hat{s})d\hat{s}$. (see 2.8)

The resonance points are ordered according to their distance s_m from the test point.

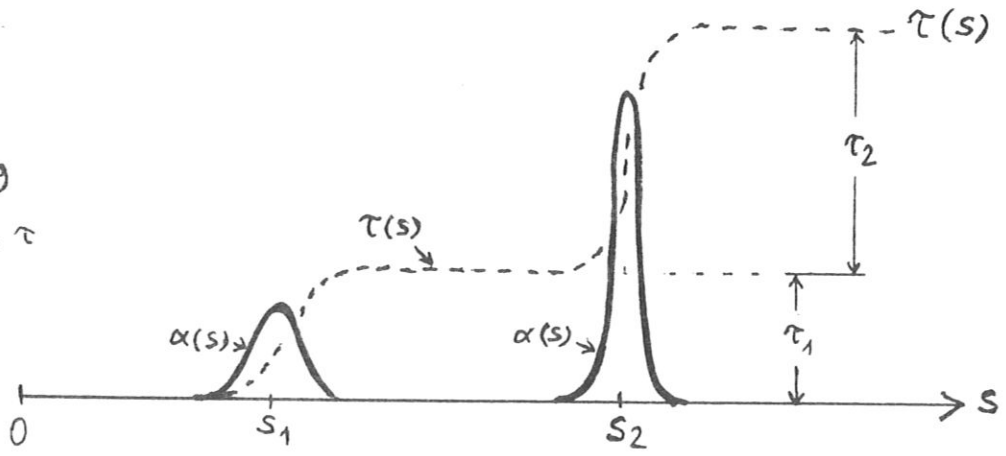

Fig. 9
α and τ

We substitute ansatz (5.1) in eq. (2.17) for the spectral function Y, (eq. (5.7)),

calculate s_m (eq. (5.9)) and τ_m (eq. (5.12)),

discuss some spectra

and determine the limits of the applicability of ansatz (5.1)

(eq. (5.19 - 21),

In this section let

the wall reflectivity be $R_{EFL} = 0$, (5.3)

the plasma current be $I_P = 0$, (5.4)

the normalization (see 2.11) be $\omega_T = \omega_H(E = R_G) = \omega_H$ on the minor axis. (5.5)

Substituting ansatz (5.1) in eq. (2.14) for the spectral function Y yields

$$\frac{Y}{\Omega_T^2} = Y_r = \int_0^{s_w} T_e(s)\, e^{-\tau(s)}\, \alpha(s)\, ds \tag{5.6}$$

$$= T_e(s_1) \int_{(s_1)} e^{-\tau(s)}\, \alpha(s)\, ds + e^{-\tau_1}\, T_e(s_2) \int_{(s_2)} e^{-\tau(s)}\, \alpha(s)\, ds \quad + \ldots$$

$$Y_r = T_e(s_1)\left[1 - e^{-\tau_1}\right] + T_e(s_2)\left[e^{-\tau_1} - e^{\tau_1 - \tau_2}\right] + \ldots \tag{5.7}$$

$$\boxed{Y_r = T_e(s_1)} \qquad \text{if } \tau_1 >> 0 \tag{5.7a}$$

The dots denote the contributions of other resonances (mostly not present). Thus, if the resonance at s_1 is opaque, Y_r denotes the electron temperature at s_1 . Now for each frequency, s_1 is located at a different point on the light path (see eq. (5.9e)). When experimentally recording a spectrum $Y(\Omega_T)$, one therefore has to

1. Choose a frequency range in which s_1 is opaque,

2. form $Y_r = Y/\Omega_T^2$,

3. convert the frequency to the distance s by means of eq. (5.9e) in order to obtain the temperature profile.

Subsidiary calculation for eq. (5.7):

$$\tau(s_1 - \varepsilon) = o$$

$$\tau(s_1 + \varepsilon) = \tau_1 \qquad \text{(see Fig. 9)}$$

$$\alpha(s)\, ds = d\tau$$

$$\int_{(s_1)} = \int_{s_1-\varepsilon}^{s_1+\varepsilon} e^{-\tau(s)}\, \alpha(s)\, ds = \int_{o}^{\tau_1} e^{-\tau}\, d\tau \qquad \text{(see eq. 2.5)}$$

We now calcule the positions S_n of the resonance points on the light path from the resonance condition

$$\omega = n\, \omega_H(S_n) \,. \tag{5.8}$$

Equation (5.8) is not exactly owing to Doppler shifting etc.
The dimensionless absorption coefficient $A(\theta, \frac{\omega}{\omega_H}, \mu)$ has its maximum near

$$\frac{\omega}{\omega_H} = n' \approx \frac{n}{1 + \frac{0,8}{\mu}(1+n)} \tag{5.8a}$$

$$\approx \frac{n}{1 + 0,00156\ (1+n)\ T_e(\text{keV})}$$

Note the difference in meaning of s_m and S_n:

the s_m are counted in terms of their distance from the test point,

the S_n in terms of the harmonics which are absorbed at the respective resonance. Substituting eqs. (2.18), (5.5), (4.11), (5.4), (3.4a), (3.3) in eq. (5.8a) yields

$$n' = \frac{\Omega_T}{R_G} \sqrt{(x_A + e_x S_n)^2 + (y_A + e_y S_n)^2} \quad . \tag{5.9a}$$

Let

$$b = \frac{x_A e_x + y_A e_y}{e_x^2 + e_y^2} \quad , \tag{5.9b}$$

$$a = \left[x_A^2 + y_A^2 - \left(\frac{n' R_G}{\Omega_T} \right)^2 \right] \Big/ (e_x^2 + e_y^2). \tag{5.9c}$$

It then follows that

$$S_n = - b \pm \sqrt{b^2 - a} \tag{5.9d}$$

In the special case $\vartheta = 90^\circ$ and $\psi = 0$ it holds that

$$S_n = \frac{1}{\cos\phi_A} \left[\left(\frac{n'}{\Omega_T} - 1 \right) R_G + R_K \cos\phi_A \right] \tag{5.9e}$$

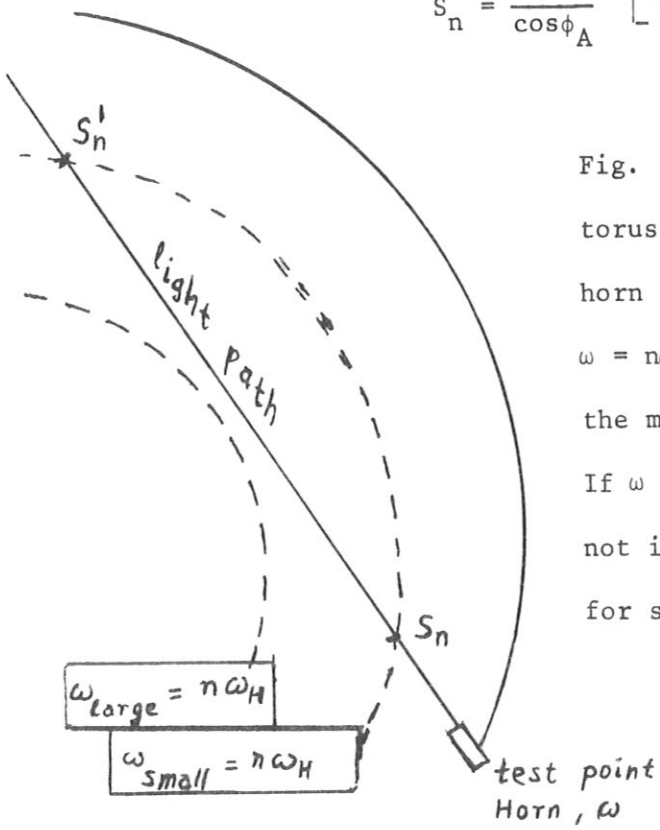

Fig. 10 shows the equatorial plane of the torus, the light path, test point, microwave horn set for the frequency ω .

$\omega = n\omega_H$ is valid for circular cylinders around the major axis.

If ω is chosen too large, the light path does not intersect the cylinder anywhere, while for small ω there are two solutions S_n and S_n'.

The s_m are obtained by ordering the S_n according to their distance from the test point.

The s_m have already been assigned the optical thickness τ_m;

the S_n are assigned the optical thickness T_n.

We calculate T_n as follows:

$$T_n = \int_{(S_n)} \alpha \, ds \quad , \tag{5.10}$$

$$T_n = \frac{\omega_p^2 (S_n)}{c\omega_H(S_n)} \int_{(S_n)} A \left(\theta(s);\ \Omega(s); \frac{511}{T_e(s)}\right) ds,$$

$$\Omega(s) = \omega / \omega_H (s) = \Omega_T \frac{E}{R_G} \quad . \tag{5.11}$$

It is now assumed that A practically only depends on s via Ω:

$$T_n = \left| \frac{ds}{d\Omega}(S_n) \right| \frac{\omega_p^2(S_n)}{c\omega_H(S_n)} \ U_n \quad , \tag{5.12}$$

$$U_n = \int_{n'-0.5}^{n'+0.5} A\left(\theta(S_n);\ \Omega;\ \frac{511}{T_e(S_n)}\right) d\Omega \quad , \tag{5.13}$$

n' see eq.(5.8a).

For $\theta = 90^o$ one has

$$U_n = U_{no} \approx \left[0{,}01\ T_e \right]^{n-1} \times \frac{\left[\frac{134.}{n-0.9} - 7. - T_e\right]^3}{1.6 \times 10^9 \times 4050^{1-n} + 2.55 \times 8.3^{8-n}} \tag{5.13a}$$

with approx. 5 - 10 % inaccuracy for $n \leq 5$; $T_e \leq 10$ keV;

If only a rough estimate (factor 2 to 3) is required, it is sufficient to take

$$U_{no} = \left[0.01\ T_e \right]^{n-1} \tag{5.13b}$$

Eq. (5.13a) may be compared with ENGELMANN's result /2/ which uses a non-relativistic approximation:

$$U_n = \frac{\pi}{2} \frac{n^{2n-1}}{(n-1)!} \left[2\mu \right]^{1-n} \sin^{2n-1} \Theta \left[1 + \cos^2 \Theta \right]$$

In rough approximation (inaccuracy approx. 50 %) it holds for

$T_e \leq 5\text{keV}$ and $\theta \geq 30^\circ$ that

$$U_n = U_{no} \sin^{2n-3}\theta \quad . \tag{5.13c}$$

Furthermore, in accordance with eqs. (5.11), (3.3), (3.4a) one has in (5.12)

$$\frac{ds}{d\Omega} = \frac{R_G}{\Omega_T} \cdot \frac{\sqrt{(x_A + e_x S_n)^2 + (y_A + e_y S_n)^2}}{e_x(x_A + e_x S_n) + e_y(y_A + e_y S_n)} \quad , \tag{5.14}$$

$$\frac{ds}{d\Omega} = \frac{R_G}{\Omega_T} \frac{1}{e_x} \qquad \text{the case } e_y = y_A = 0 \quad . \tag{5.14a}$$

Before discussing the spectra, let us estimate the orders of magnitude expected for one example (JET):

Data (JET)

$D_M = 10^{14}\,\text{cm}^{-3}$

$H_T = 31.\text{kG}$

$R_G = 290$ cm

$R_K = 130$ cm

$T_M = 3\text{keV}$

$\phi_A = \pi$

$\vartheta = \pi/2$

$\psi = 0$

Conclusions

$$\omega_p = \sqrt{\frac{4\pi}{m_e} e^2 D_M} = 5.6 \times 10^{11}\ \text{sec}^{-1} \tag{5.15}$$

$$\omega_T = \frac{e}{m_e c} H_T = 5.4 \times 10^{11}\ \text{sec}^{-1} \tag{5.16}$$

$$\frac{\omega_p^2}{c\omega_H} = 20$$

On the minor axis one has

$$T_n = \frac{6000}{\Omega T} U_n$$

$$T_n = 3000 U_n \text{ for } \Omega_T = 2 \tag{5.16a}$$

The first two resonances are thus completely opaque, T_3 is semi-opaque etc.

n	U_{no}	T_n (eq. (5.16a))
1	1,5	4500.
2	0,034	100.
3	$1,4\ 10^{-3}$	4.
4	$8,2\ 10^{-5}$	0,2
5	$6,2\ 10^{-6}$	0,02

table I

Fig. 11

Light path in example (5.15)

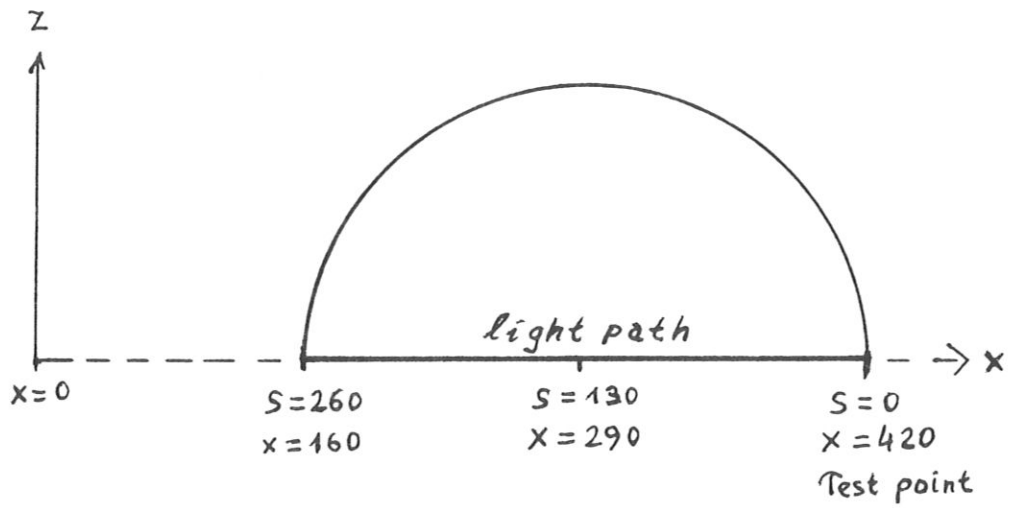

Fig. 12

Position of resonances

on the light path

in Fig. 11

for 3 frequencies.

Data:

$D_M = 10^{14} cm^{-3}$

H_T = 31.kG

P_D = 0 (box shape)

P_T = 2 (bell shape)

R_G = 290 cm

R_K = 130 cm

T_M = 3keV

$\phi_A = \pi$

$\vartheta = \pi/2$

$\psi = 0$

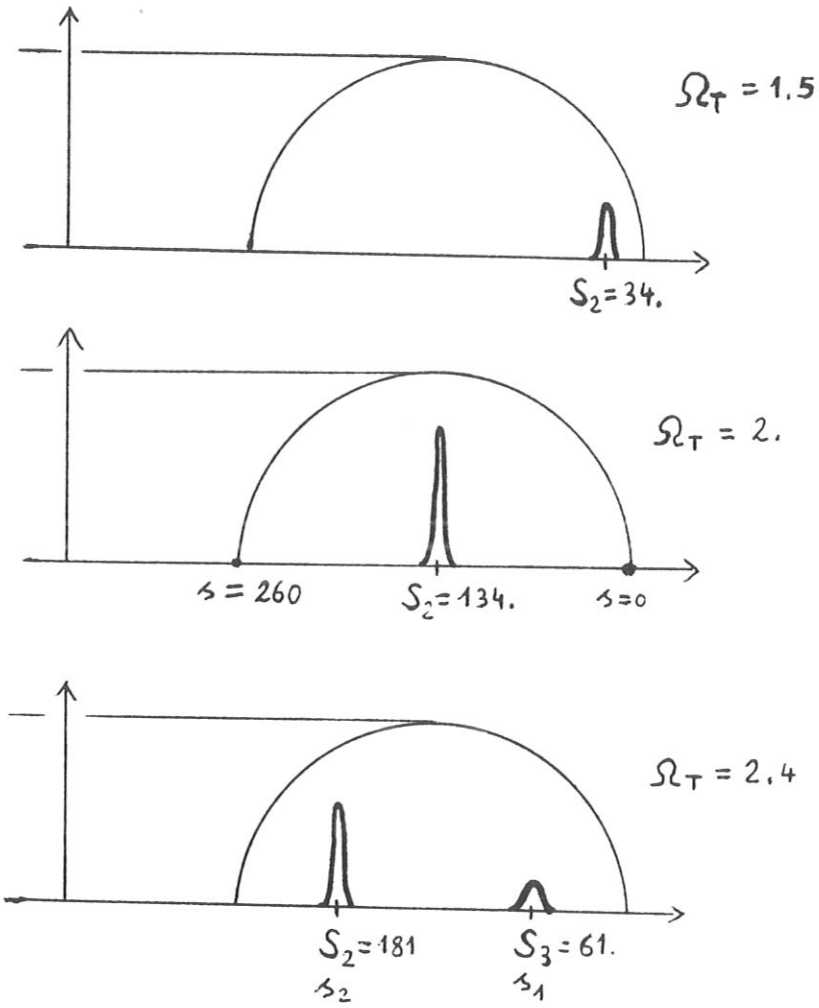

The S_n and s_m

are plotted

for Ω_T = 2.4.

Fig. 13

Spectrum Y versus Ω_T

for the data

in Fig. 12

and RAYLEIGH JEANS

parabola

(see list p. 66)

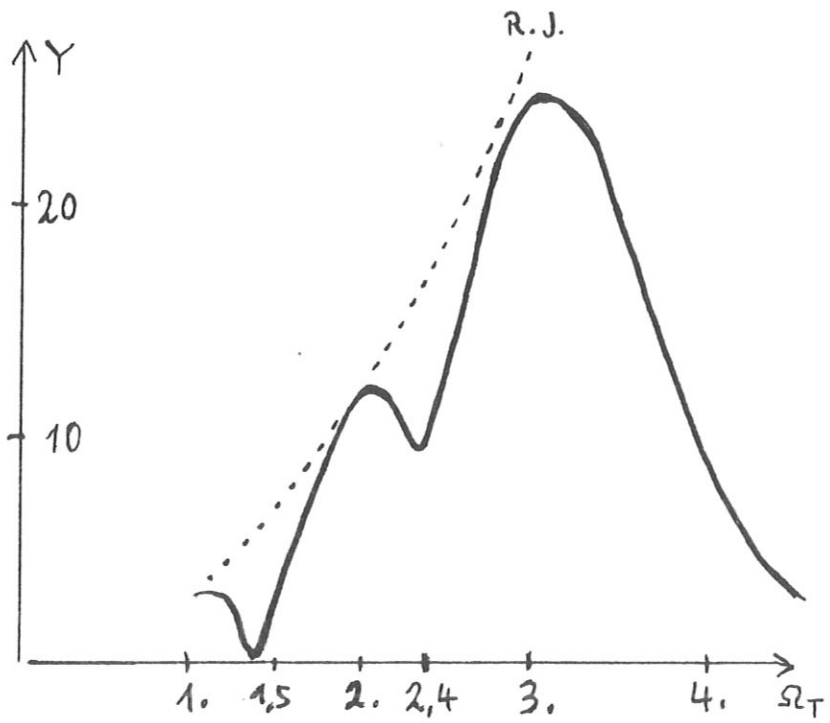

Fig. 12 is not true to scale.

The resonance widths in Fig. 12 are a few cm (see eq. (5.21)); on the scale of Fig. 12 (1 : 50) this is $\lesssim$ 1 mm, i.e. the resonances would scarcely identifiable if they had been plotted true to scale versus s.

For $\Omega_T = 2.4$ there are two resonance points. In this case one has approximately

$$\omega \approx 2\omega_H(s = 181) \approx 3\omega_H(s = 61) \qquad \text{(see 5.8a)}$$

Physically, this means that the electrons located at s = 181 gyrate about one and a half times as fast as the electrons located at s = 61. The frequency ω for $\Omega_T = 2.4$ corresponds to the 2nd harmonic (n = 2) at s = 181 and also to the 3rd harmonic (n = 3) at s = 61.

From $p_T = 2$ it follows that the temperature at s = 61 is only $T_e(61) = 1{,}4$keV. Consequently, the optical thickness is $T_3(61) = 1.2$; (see p. 66) owing to $e^{-1.2} = 0.3$ it follows that only 30 % of the light generated by s = 181 reaches test point, the rest being absorbed at s = 61. The frequency range around $\Omega_T = 2.3 - 2.4$ is a transition region in which the radiation contributions of the n = 2 and the n = 3 resonance are superposed.

For comparison it should be noted that a sun glasses lens which transmits 1/8 of the incident light has optical thickness depth $\tau = \ln 8 = 2.1$.

For $\Omega_T = 2$ the resonance $s_2 = 134$ is shifted away from the minor axis (s = 130) proportional to $n' - n$.

The plasma layers for which it holds that $\omega = n\omega_H$ absorb light like sun glasses; but they also emit as well.

In the region $1.4 \leq \Omega_T \leq 2.3$ (5.17)

one has $$Y_r = \frac{Y}{\Omega_T^2} = T_e(S_2) \qquad (5.7a)$$

The fact that the optical thickness T_2 of the n = 2 resonance is very large relative to unity means that the resonance points on the left of the n = 2 resonance in Fig. 12, which are not covered by our theory (hybrid frequency, plasma frequency etc.), are not visible to an observer at the test point. We therefore expect eq. (5.7a) to remain valid in the region (5.17) when using a refined theory which takes the influence of the plasma on the dielectric constant and the refractive index into account.

The decrease of Y for higher frequencies is due to the effective higher resonances (n = 4, n = 5) being much weaker; see table I for the case (5.15).

In Fig. 14 we investigate the influence of the temperature T_M in the centre (minor axis) on the spectra. The optical thickness T_3 of the 3rd resonance depends very strongly on the temperature. In the transition region around $\Omega_T \simeq 2.4$,

T_3 is opaque at 5keV and therefore $Y_r = T_e(S_3) \simeq 0.3\ T_M$, while it is transparent at 1 keV and therefore $Y_r = T_e(S_2) \simeq 0.6\ T_M$.

The minimum located at $\Omega_T = 2.4$ can therefore hardly be identified at 1 keV. At 5 keV the n = 4 resonance also makes appreciable contributions; hence the dip at $\Omega_T = 3.5$.

In Fig. 15 we investigate the influence of the temperature <u>profile</u> on the spectra. In the vicinity of $\Omega_T = 2.2$ one has $Y(p_T = 2) > Y(p_T = 1)$, because the n = 3 resonance located at $S_3 = 65$ is more transparent in the case $p_T = 2$ than in the case $p_T = 1$. The jagged edges observed for $Y(p_T = 0)$ are caused

at $\Omega = 3.5$ by the vanishing of the n = 2 resonance

and at $\Omega = 5.4$ by the vanishing of the n = 3 resonance.

The straight part for $\Omega_T \geq 5.4$ is thus the contribution of the n = 4 resonance; the contributions of the higher resonances are negligible.

The term "vanishing" means the following:

If Ω_T is gradually increased, the n = 2 resonance (see Fig. 12) moves (to the left in this case) and vanishes for $\Omega_T = 3.5$ on the left at s = 260.

With cylinder-like spectra - in general, when the resonance width is larger than the light path length - the line profile has completely different causes, which are discussed in §6.

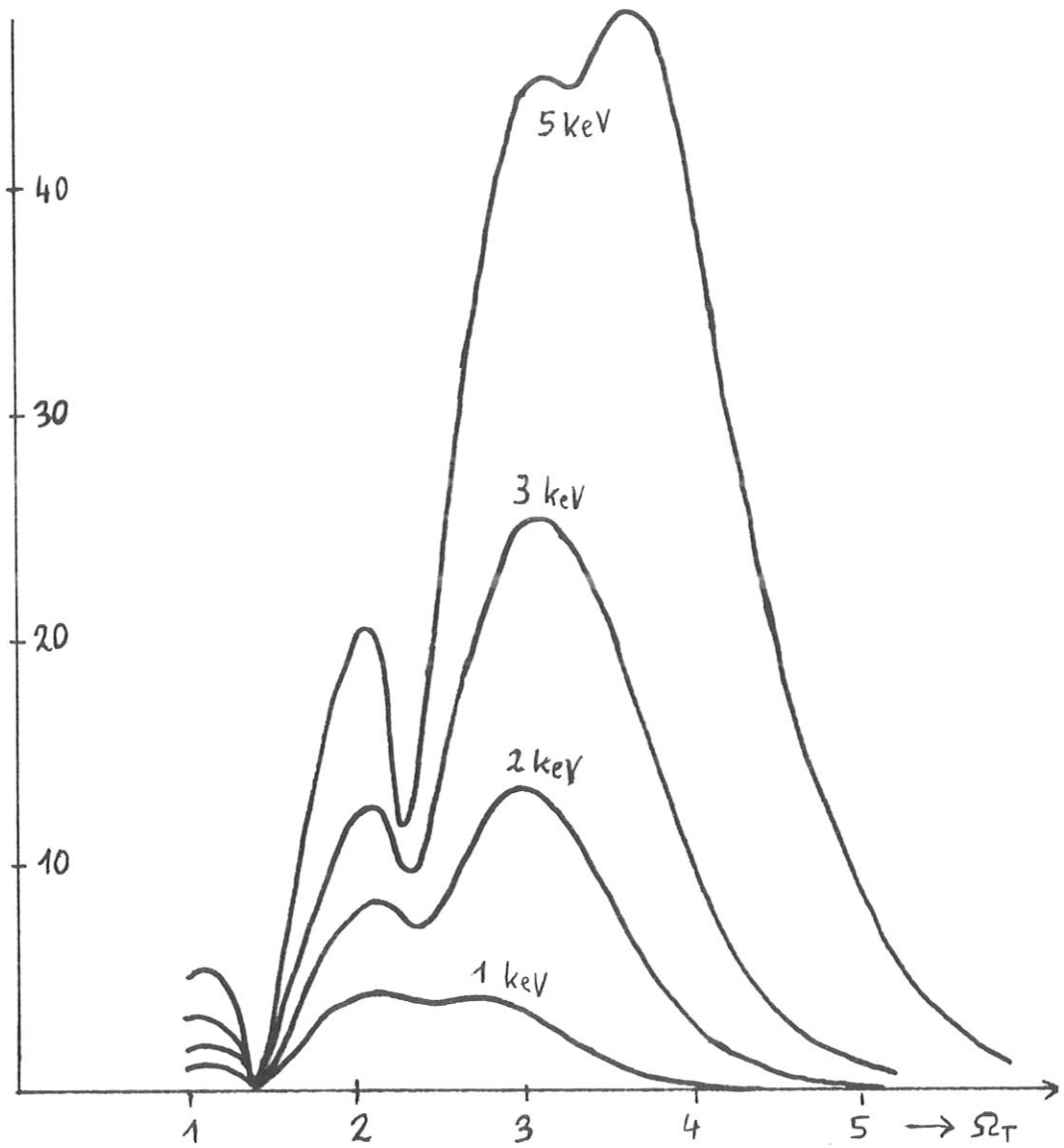

Fig. 14

Spectra Y versus Ω_T.

T_M is varied.

ϑ = 1.57

ψ = 0.

$D_M = 10^{14} cm^{-3}$

H_T = 31.kG

ϕ_A = 3.14

P_D = 0.

P_T = 2

R_{EFL} = 0

R_G = 290.cm

R_K = 130.cm

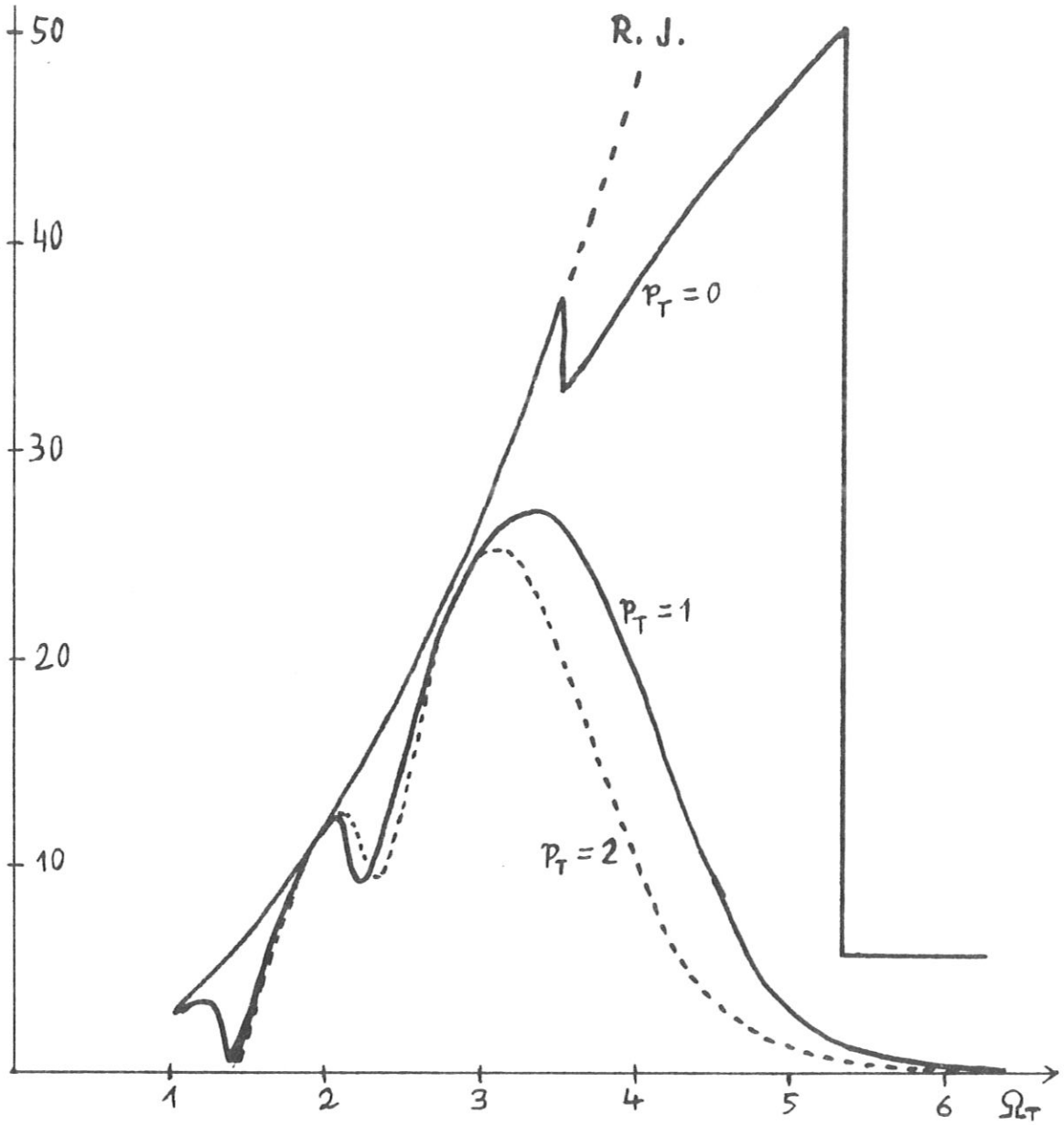

Fig. 15
Spectra Y versus Ω_T.
The temperature profile number p_T is varied.

ϑ = 1.57
ψ = 0.
$D_M = 10^{14}\,cm^{-3}$
H_T = 31.kG
ϕ_A = 3.14
P_D = 0
R_{EFL} = 0
R_G = 290. cm
R_K = 130. cm
T_M = 3.keV

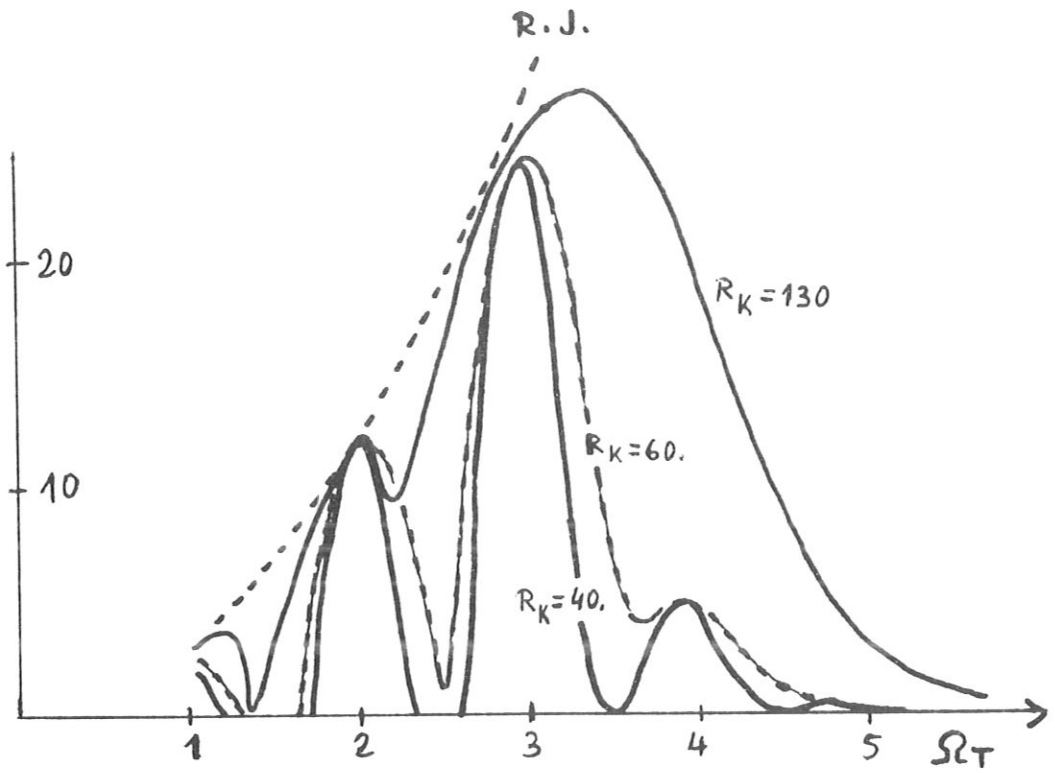

Fig. 16

Spectra Y versus Ω_T.

The minor radius is varied. R.J. is the RAYLEIGH-JEANS parabola. If R_K is reduced (or R_G increased), one sees lines in the vicinity of integral values of Ω_T. These lines become narrower as R_K/R_G is decreased. As long as the resonance width (eq. (5.21)) is small relative to the light path length s_w, the line profile essentially reproduces the temperature distribution (eq. (5.7a)).

Parameters:

$\vartheta = 1.57$

$\Psi = 0$

$\Phi_A = 3.14$

$D_M = 10^{14}\,cm^{-3}$

$H_T = 31.\ kG$

$p_D = 0$

$p_T = 1$

$R_{EFL} = 0$

$R_G = 290.\,cm$

$T_M = 3.\,keV$

Finally, let us make a few remarks on the range of validity of the δ approximation (eq. (5.1)).

Equation (5.1) is valid when the resonance width is small relative to the light path length s_w:

$$\Delta s \ll s_w \tag{5.19}$$

First we define and calculate the resonance width:

The "resonance width" is the interval in which the emissivity is essentially $\neq 0$.

According to KIRCHHOFFS's law (2.14) the emissivity is proportional to the absorption coefficient; this, in turn, depends by way of $\theta(s)$, $\Omega(s)$ and $T_e(s)$ on the parameters of eq. (2.19). It is found that A as a function of Ω shows sharp resonance lines if T_e is a few keV and θ is not too far from 90°. According to ENGELMANN /2/ the resonance width is given in rough approximation by

$$\Delta\Omega = \sqrt{\frac{2\pi}{\mu}}\, n \left\{ \cos\theta + \sqrt{\frac{n}{\mu}} \right\}, \tag{5.20}$$

where the formulae for $\theta = 90^\circ$ and $\theta \neq 90^\circ$ are arbitrarily combined to make one formula;

$$\mu = \frac{511}{T_e(\mathrm{keV})} \quad . \tag{2.14}$$

By means of eq. (5.14) we change from the frequency resonance width to the light path resonance width:

$$\Delta s = \frac{ds}{d\Omega}\, \Delta\Omega \tag{5.21}$$

$$\Delta s = \frac{ds}{d\Omega}\,\Delta\Omega \tag{5.21}$$

Example: Fig. 12

$$\frac{ds}{d\Omega} = 150 \text{ cm (for } \Omega_T = 2),$$

$$\Delta\Omega = \sqrt{2\pi}\,\frac{n^{3/2}}{\mu} = 0{,}08 \text{ for } n = 3,\ T_e = 3\text{keV},$$

$$s = 12 \text{ cm},$$

§6 Profile ansatz for A

In cylindrical geometry - but also in toroidal geometry at $\phi_A = 90^o$ or at high temperatures and frequencies - the resonance width is larger than the light path length:

$$\Delta s > s_w . \tag{6.1}$$

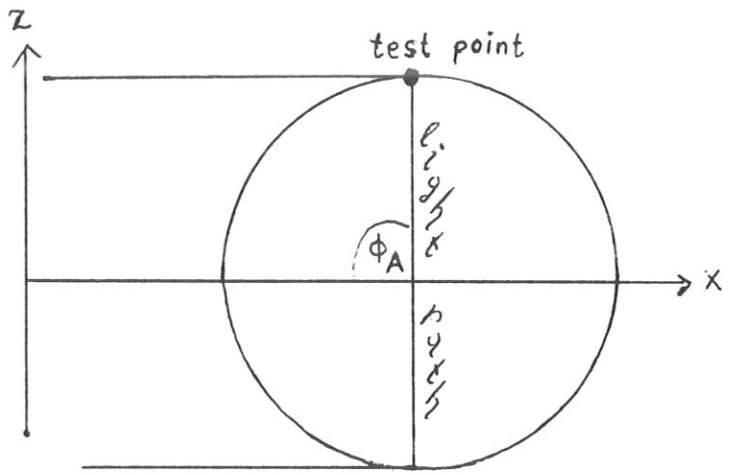

Fig.17 shows the test point and light path in toroidal geometry for

$\vartheta = 90^o$

$\psi = 0$

$\phi_A = 90^o$.

In such cases the absorption coefficient A is often given in more or less rough approximation by a profile ansatz of the same type as eq. (4.1):

$$A = A_M(1-\hat{r}^2)^{p_A} . \tag{6.2}$$

In cylindrical geometry one has $\theta = \vartheta$ and $A_M = A(\theta\ ;\ \Omega;\ \frac{511}{T_M})$. (6.2a)

In toroidal geometry and with $\vartheta = 90^o$ one has $A_M = A(\frac{\pi}{2};\ \Omega;\ \frac{511}{T_M})$. (6.2b)

Ansatz (6.2) is substituted in eq. (2.17) for the spectral function Y. The integration may be carried out in analytic approximation (eqs. (6.3) - (6.8)). This is conditional upon

(6.2a) cylindrical geometry or

(6.2b) toroidal geometry and $\vartheta = 90^{\circ}$ being satisfied, so that one has

$$1-\hat{r}^2 = \hat{s}\left[\,2\cos\psi - \hat{s}\,\right] . \tag{6.3}$$

with $$\hat{s} = \frac{s}{R_K}\sin\theta \quad .$$

Let

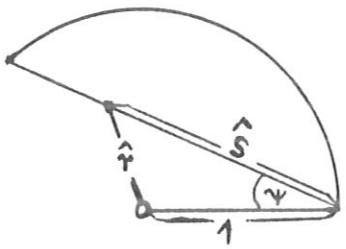

$$M = p_A + p_D \tag{6.4a}$$

$$P = p_A + p_D + p_T \tag{6.4b}$$

$$\tau_D = \frac{1}{\sin\theta}\, A_M\, D\, (\cos\psi)^{2M+1} \tag{6.4c}$$

$$D = \frac{\omega_M^2 R_K}{c\,\omega_H} \qquad (\text{see } 4.18) \tag{6.4d}$$

$$\omega_p^2 = \omega_M^2 (1-\hat{r}^2)^{p_D} \tag{6.4e}$$

ω_H independent of s. (6.1)

It then follows that

$$Y_r = \frac{Y}{\Omega_T^2} = T_M \cdot I_o (\cos\psi)^{2p_T} . \tag{6.5a}$$

In cylindrical geometry it is even possible to take the wall reflection into account in a simple form (see §7, eq. (7.16)):

$$Y_r = T_M \cdot I_o (\cos\psi)^{2p_T} \Big/ \left[\,1-R_{EFL}\, e^{-\tau_c}\,\right] \tag{6.5b}$$

where

$$\tau_c = \tau_D \int_0^2 (2\xi - \xi^2)^M d\xi \approx \frac{2\tau_D}{\sqrt{1+1.26\ M}} \tag{6.6}$$

$$I_o = \tau_D \int_0^2 (2\xi - \xi^2)^P e^{-\tau} d\xi \approx \frac{1-e^{-\tau_p}}{(1+0.3\tau_p)^E} \tag{6.7}$$

$$\tau = \tau_D \int_0^\xi (2\rho - \rho^2)^M d\rho$$

$$\tau_p \approx \frac{2\tau_D}{\sqrt{1+1.26\ P}}$$

$$E = \frac{(P-M)^{0.9}}{(0.85 + M)^{1.086}}$$

The inaccuracy of the approximations is:

in eq. (6.6) about 0.5 %

in eq. (6.7) about $(0.5 + 2p_T)$ %, i.e. 1 to 5 %.

Compared to the previous section (eq. (5.7a)) the essential difference is the denominator in eq. (6.7), which keeps I_o and hence Y_r low for large τ, so that I_o and Y_r attain their maxima at medium τ values (see Fig. 18).

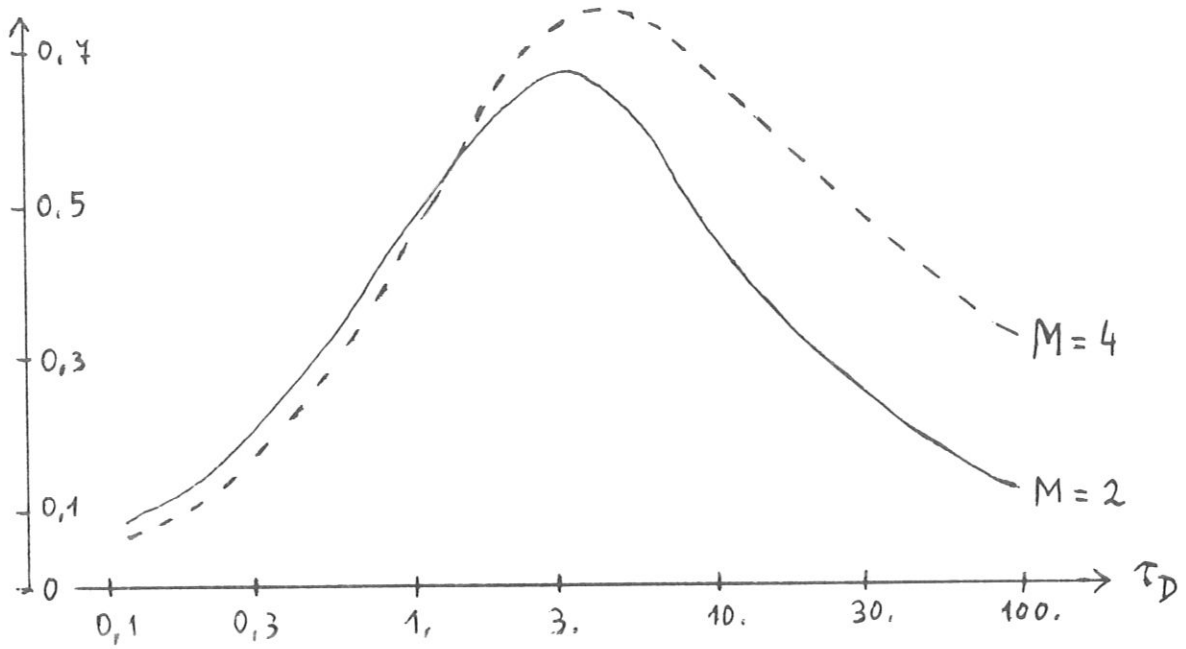

Fig. 18

I_o plotted versus τ_D for $p_T = 2$ (bell-shaped temperature profile) and two different density profiles.

We now turn to the physical interpretation:

According to eq. (6.4a) M = 2 gives a blunter density profile than M = 4. Owing to $p_T = 2$ the plasma boundary layers are cooler than in the centre, and in the case M = 2 denser than in the case M = 4, so that in the case M = 2 more of the radiation emitted from the hot interior is absorbed. At large optical depths τ_D less reaches the test point for M = 2, so that I_o and Y_r are smaller than in the case M = 4. For very small optical depths there is more radiating plasma present in the case M = 2, and I_o is therefore a little larger than for M = 4. It can thus be generally stated that the cyclotron emission is strongest when the plasma is semi-opaque, i.e. not too opaque but not too transparent either:

$$1 \lesssim \tau_D \lesssim 10. \tag{6.9}$$

It should be noted that eq.(6.9) is a property of temperature profiles in which the plasma is hotter inside than outside ($p_T > 0$). With a box-shaped temperature profile ($p_T = 0$) I_o increases monotonically with increasing τ_D:

$$\lim_{\tau_D \to \infty} I_o \to 1 \qquad \text{for} \quad p_T = 0 \tag{6.10}$$

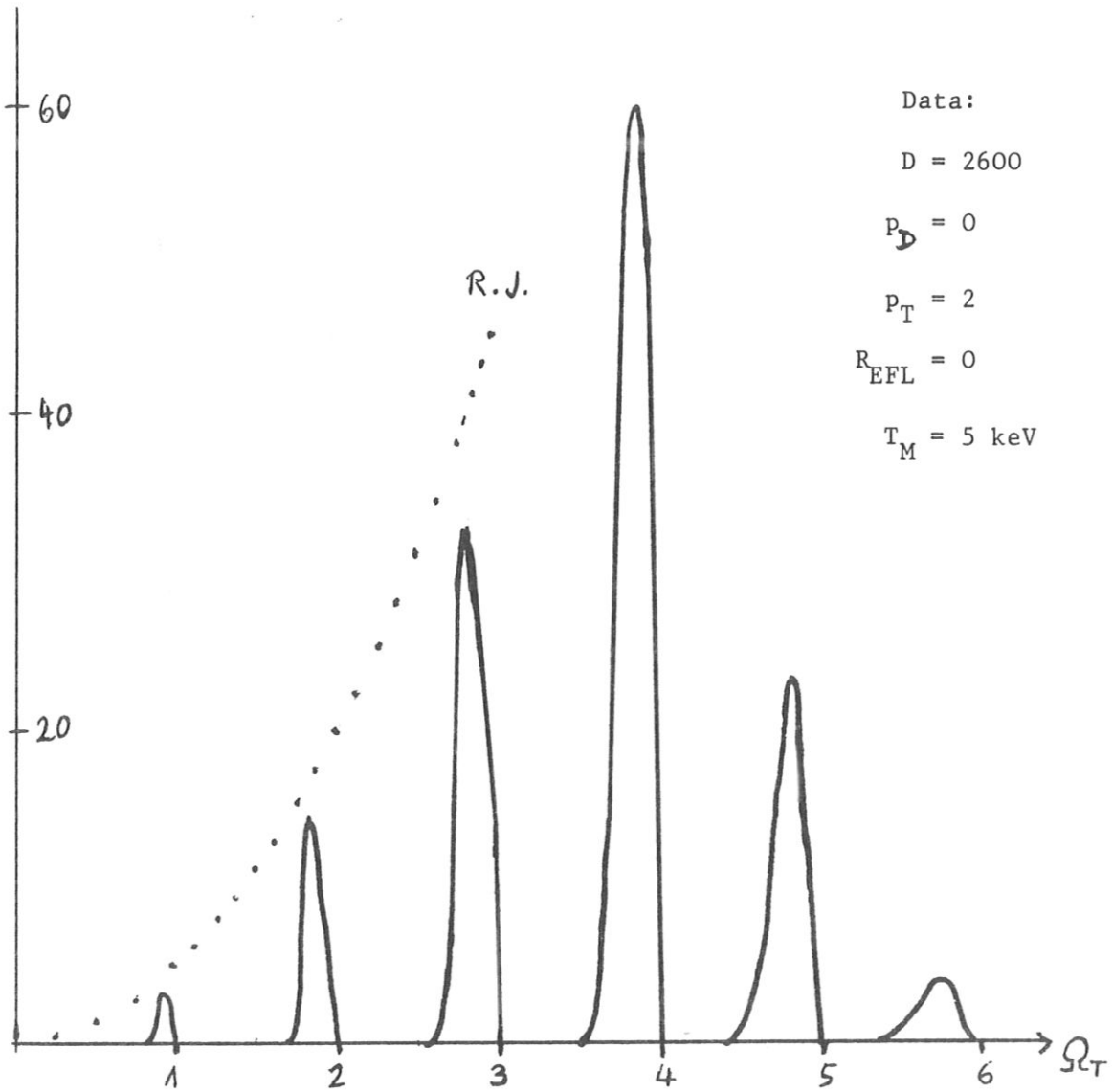

Fig. 19

Spectrum Y versus Ω_T

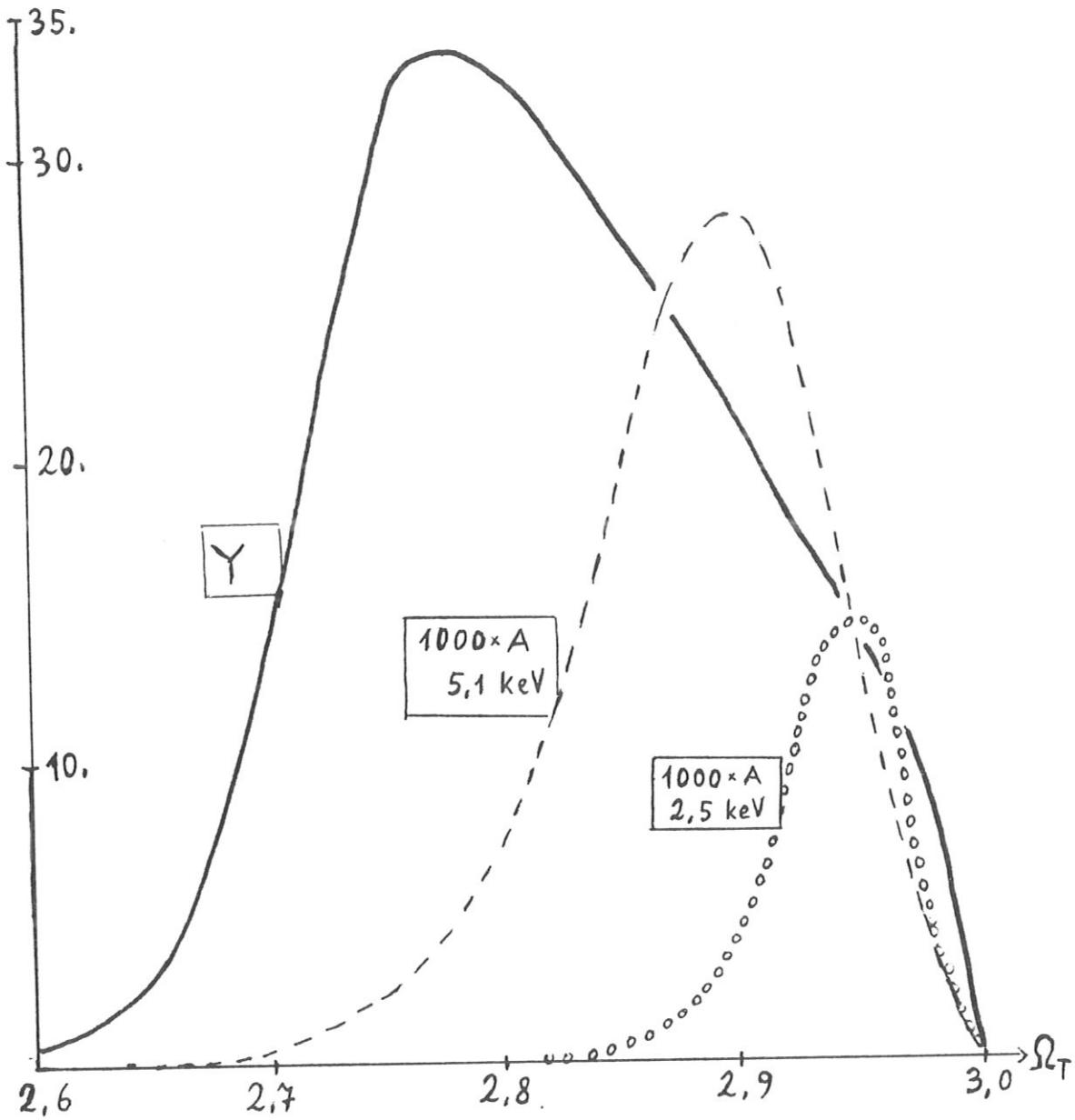

Fig. 20

The 3rd harmonic of the spectral function Y from Fig. 19, highly enlarged.

Data: D = 2600; p_D = 0; p_T = 2; T_M = 5keV; $\Theta = 90^o$; $\psi = 0^o$.

Also given for comparison is the dimensionless absorption coefficient A ($\Theta = 90^o$; Ω_T; $\frac{511}{5.1}$)

and A($\Theta = 90^o$; Ω_T; $\frac{511}{2.5}$) .

To calculate the spectra in Fig. 19 to 21, eq. (2.17) was numerically integrated by means of suitably chosen gridpoints for s. We now qualitatively interpret the curves by means of eq. (6.9).
Figure 20 shows the 3rd harmonic, highly enlarged, from Fig. 19; also shown for comparison is the dimensionless absorption coefficient A.
In accordance with eq. (6.4c) it follows that

$$\tau_D = A_M D \ .$$

Equation (6.9) is best satisfied for $\Omega_T \approx 2.8$; the cyclotron emission Y is therefore strongest at $\Omega_T \approx 2.8$. At $\Omega_T = 2.9$, A and hence τ_D have their maxima; the value of τ_D there is $\tau_D = AD = 70$; according to Fig. 18 I_o and hence Y have dropped there to about half their maximum values. At $\Omega_T = 2.97$ there is also an interval in which eq. (6.9) is satisfied. One should therefore expect a further maximum of Y, i.e. the Y line should split into two components; as Table II shows:

Table II

Ω_T	τ_D	I_o(Fig. 18)	Y(eq.6.5)	Y(Fig. 20)
2.75	7.	0.6	30.	35.
2.9	70.	0.2	15.	20.
2.97	10.	0.5	25.	10.

Such splitting into components if often found in cylindrical spectra, particularly at oblique angles (Fig. 21), where the profile ansatz (6.1) for A is very good approximation. In Fig. 20 this is not so because A in the vicinity of $\Omega_T = 2.97$ cannot even approximately be described by a profile ansatz, as the comparison of the two curves for A shows.
It is thus found that the maximum of the spectral function Y is shifted

much further to the left than would be expected from the pure DOPPLER shift (see maximum of A). This is due to the greater transparency of the plasma to the frequencies emitted by the high-energy tail of the MAXWELL distribution (in Fig. 20: around Ω_T = 2.75 - 2.80).

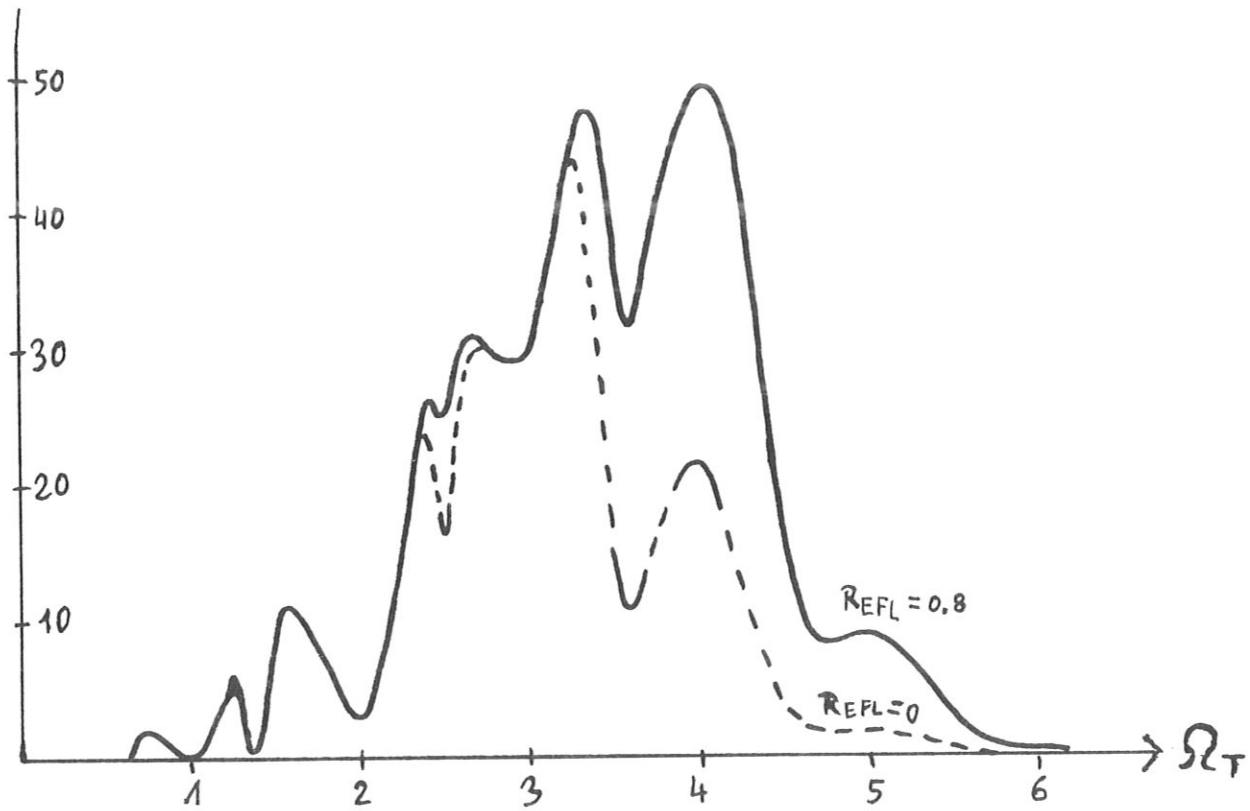

Fig. 21

Spectra Y versus Ω_T for cylindrical geometry

with and without wall reflection.

The lines n = 1, 2, 3 split into two components,
the lines n = 4, 5 do not split because τ_D is too small there.
It is also seen how the wall reflectivity shifts the cyclotron emission to higher frequencies.
Parameters: D = 3000.
$p_D = p_T = 1$
T_M = 5 keV
ψ = 0
θ = 0,77 = 44°

§7 Reflecting walls

Let the inner surface of the torus be smooth as a mirror and reflect the fraction $R_{EFL} < 1$ of the incident light into the plasma.

R_{EFL} denotes the "reflectivity of the wall". Mostly it has a value of

$$R_{EFL} \approx 0.9. \tag{7.1}$$

The consequences of this are illustrated in Fig. 22. The test point receives light not only from the light path between the test point and R_1, already treated in §2 - 5, but also,
after single reflection, from the light path R_2R_1, and then,
after double reflection, from the light path R_3R_2, etc.

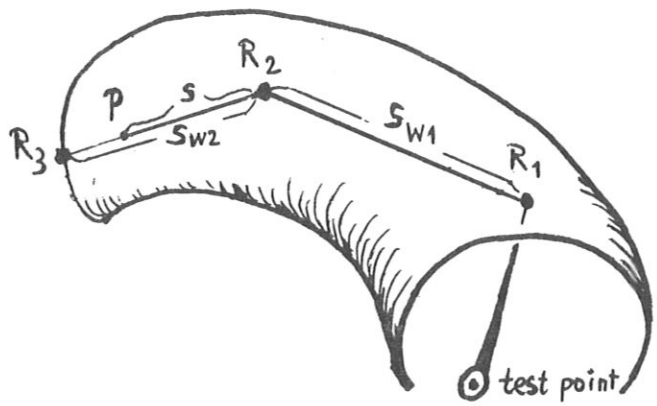

Fig. 22
Torus segment
(in perspective)
3 light paths,
3 reflection points

Every time the light is reflected from the wall it becomes weaker by the factor R_{EFL}. The contribution of the plasma element located at P (Fig. 22) to the intensity at the test point is therefore

$$R_{EFL}^2 \, e^{-\tau_P} \, \alpha(P) \, T_e(P) \, , \tag{7.2}$$

where $\alpha(P) = \alpha$ at the point P etc.

τ_P = optical depth of the <u>total</u> path P-R_2-R_1-test point.

For quantitative description we assign:

the light path "test point-R_1" the index N = 0

the light path R_1-R_2 the index N = 1

the light path R_2-R_3 the index N = 2, etc.

Let the test point have the Cartesian coordinates x_o, y_o, z_o,

Let R_1 have the Cartesian coordinates x_1, y_1, z_1,

Let R_2 have the Cartesian coordinates x_2, y_2, z_2,

etc. s = the distance from R_N (see Fig. 21).

Let the direction of the light path "test point-R_1" be e_{xo}, e_{yo}, e_{zo},

Let the direction of the light path R_1-R_2 be e_{x1}, e_{y1}, e_{z1},

etc.

According to eqs. (3.3) and (3.4) the distance of the point s from the major axis is then

$$E_N(s) = \sqrt{(x_N + e_{xN}s)^2 + (y_N + e_{yN}s)^2} \tag{7.3}$$

and, furthermore, the distance of the point s from the minor axis is

$$r_N(s) = \sqrt{(R_G - E_N(s))^2 + (z_N + e_{zN}s)^2}. \tag{7.4}$$

According to eq. (4.2) one has

$$T_{eN}(s) = T_M(1-\hat{r}_N^2)^{p_T}, \tag{7.5}$$

where the subscript N is necessary because

$$\hat{r}_N = r_N(s)/R_K \tag{7.6}$$

depends on N.

According to eq. (2.19) one has

$$\alpha_N(s) = \frac{\omega_{pN}^2(s)}{c\omega_{HN}(s)} \cdot A\left(\theta_N(s); \frac{\omega}{\omega_{HN}(s)}; \frac{511}{T_{eN}(s)}\right) , \tag{7.7}$$

$$\omega_{pN}^2(s) = \omega_M^2 (1-\hat{r}_N^2)^{P_D} , \tag{7.8}$$

$$\omega_{HN}(s) = \omega_T R_G / E_N(s) , \tag{7.9}$$

$$\tau_N(s) = \int_0^S \alpha_N(\hat{s})\, d\hat{s} , \tag{7.10}$$

$$\tau_{NC} = \sum_{K=0}^{N-1} \tau_K(S_{WN}) \tag{7.11}$$

$$\tau_{OC} = 0.$$

S_{WN} = length of the light path N.

According to eq. (7.2) it then follows that

$$Y_r = Y/\Omega_T^2 = \sum_{N=0}^{\infty} R_{EFL}^N e^{-\tau_{NC}} \int_0^{S_{WN}} e^{-\tau_N(s)} \alpha_N(s)\, T_{eN}(s)\, ds. \tag{7.12}$$

This still leaves the determination of the coordinates x_N, y_N, z_N and the directions e_{xN}, e_{yN}, e_{zN}. The x_N, y_N, z_N are numerically determined according to eq. (3.7), while the directions are determined from the reflection law:

It is assumed that the direction of the light path N-1 is known; for N=0 see eq. (3.2).

Let $\vec{e}_{N-1} = \vec{e}$ = direction of light path N-1;

Let $\vec{e}_N = \vec{c}$ = direction of light path N;

Let $\vec{f}$ = direction of surface normal in $R_N = (x_N, y_N, z_N)$.

From the equation

$$R_K^2 = (R_G - \sqrt{x^2 + y^2})^2 + z^2 \tag{7.13}$$

for the torus surface it follows that

$$f_x = \frac{\frac{\partial}{\partial x} R_K^2}{\sqrt{\left[\frac{\partial}{\partial x}(R_K^2)\right]^2 + \left[\frac{\partial}{\partial y}(R_K^2)\right]^2 + \left[\frac{\partial}{\partial z}(R_K^2)\right]^2}}$$

f_y and f_z are obtained by analogy. After differentiation, we replace x by x_N etc.

Let

$$g = 1 - \frac{R_G}{\sqrt{x_N^2 + y_N^2}} \quad , \tag{7.14a}$$

$$w = \sqrt{(gx_N)^2 + (gy_N)^2 + z_N^2} \, . \tag{7.14b}$$

It then follows that

$$f_x = gx_N/w \quad , \tag{7.14c}$$

$$f_y = gy_N/w \quad , \tag{7.14d}$$

$$f_z = z_N/w \quad . \tag{7.14e}$$

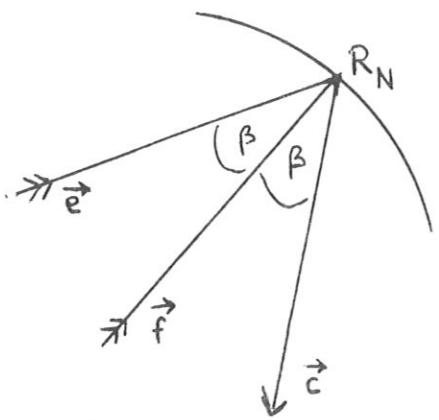

Fig. 23

In addition, let

u = cosß (see Fig. 23), and hence

$u = (\vec{e}.\vec{f})$.

From the reflection law it then follows that

$$(\vec{c}.\vec{f}) = -u = \cos ß \tag{7.15a}$$

$$(\vec{c}.\vec{e}) = 1 - 2u^2 = -\cos(2ß) \tag{7.15b}$$

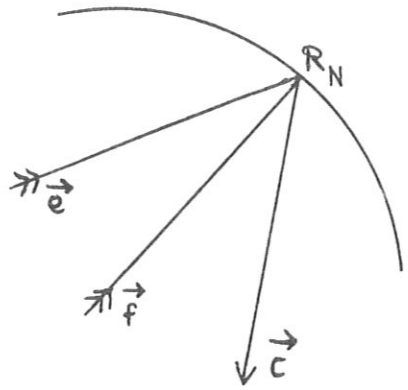

The minus sign occurs because $\vec{c}$ points inwards, but $\vec{e}$ and $\vec{f}$ outwards.

By means of the vectors

$$\vec{D} = \left[\vec{e} \times \vec{f}\right] \quad , \tag{7.15c}$$

$$\vec{Q} = u\vec{e} + (1-2u^2)\vec{f} \tag{7.15d}$$

$\vec{c}$ can be expressed in the form

$$\vec{c} = \frac{1}{D^2}\left[\vec{Q} \times \vec{D}\right] \quad . \tag{7.15e}$$

This gives us all the formulae required for programming Y.

In cylindrical and slab geometry the contributions of the light paths are equal, thus making the subscript N superfluous.

Equation (7.12) simplifies to

$$Y_r = \frac{\int_0^{S_W} \alpha(s)\, e^{-\tau(s)} T_e(s)\, ds}{1 - R_{EFL}\, e^{-\tau_c}} \quad . \tag{7.16}$$

It can be generally stated that:

As a result of wall reflection the maximum of the cyclotron emission is shifted to higher frequencies because the plasma is rather transparent there and, consequently, one can see the wall reflections from the test point, whereas at low frequencies the plasma is usually opaque.

In addition, it should be noted that the formulae (7.1-16) refer to the intensity at the inner side, where the radiation intensity is amplified by the wall reflection; the cyclotron radiation losses are

a factor of $(1-R_{EFL})$ smaller:

$$Y_{out} = (1-R_{EFL})\ Y \tag{7.17}$$

where Y_{out} denotes Y at the outer side .

Subsidiary calculation for eq. (7.10-12)

$$Y_T = \int_0^{s_{W0}} e^{-\tau_0(s)}\ \alpha_0(s)\ T_{e0}(s)\ ds$$

$$+ R_{EFL}\ e^{-\tau_{1C}} \int_0^{s_{W1}} e^{-\tau_1(s)}\ \alpha_1(s)\ T_{e1}(s)\ ds$$

$$+ R_{EFL}^2\ e^{-\tau_{2C}} \int_0^{s_{W2}} e^{-\tau_2(s)}\ \alpha_2(s)\ T_{e2}(s)\ ds$$

$$+ \ldots$$

For the τ_p from eq. (7.2), fig. 21, one has

$$\tau_p = \tau_2(s) + \tau_1(s_{W1}) + \tau_0(s_{W0})$$

$$\tau_{1C}$$

$$\tau_{2C}$$

§8 Approximation formula for the intensity

The intensity of the cyclotron radiation of the plasma cylinder is

$$\frac{\partial^2 E}{\partial S \partial t} = m_e \omega_H^3 I \qquad (\omega_H = \omega_T = \text{const}) \qquad \text{(see (2.15))}$$

The numerical results can be given in the following form with an inaccuracy of about 10 %:

$$I = I_{cyl} = 1.5 \times 10^{-5} T_M^2 (1 + 0{,}022 T_M) (\frac{D}{1000})^{\hat{E}} R \hat{P} \quad , \qquad (8.1)$$

where

$$\hat{E} = 0{,}23 + 0{,}07 T_M^{1/3} \cdot (7.4 + 3.47 \ln T_M) \frac{\ln(\frac{D}{1000})}{1000} \quad , \qquad (8.2)$$

$$R = (1.-R_{EFL})^S \quad , \qquad (8.3)$$

$$S = -0.32 - \frac{0.68}{(1+D)^{0.7}} - 0.0013 T_M \approx -0.33 \quad , \qquad (8.4)$$

$$\hat{P} = (0{,}13 + 0{,}87 p_T)^{-0.61} \quad , \qquad (8.5)$$

$$D = \frac{\omega_M^2}{c\omega_H} R_K \qquad \omega_M = \text{plasma frequency at the cylinder axis} \qquad \text{(see (6.4d)} \quad ,$$

T_M = temperature on the cylinder axis in keV,

$$P_D = P_T \quad . \qquad (8.6)$$

At $p_D - p_T \approx 1$ to 2, I increases by about 2 %. (8.7)

Ranges of application:

$$\begin{aligned} 1\ \text{keV} \lesssim T_M &< 100\ \text{keV} \quad , \\ 0{,}1 \quad < D &< 10^5 \quad , \\ 0 \quad \lesssim R_{EFL} &< 0{,}99 \quad , \\ 0 \quad \lesssim p_T &< 3 \text{ to } 4 \quad . \end{aligned} \tag{8.8}$$

For very small D (at T_e = 100 keV about $D \leq 0.3$) there is only very little reabsorption, and hence I is proportional to D, i.e.

$\hat{E} = 1$ is the largest possible $\hat{E}$ value. (8.2a)

In eq. (8.1) I denotes the intensity on the "inner" side, i.e. on the side of the wall facing the plasma. The intensity on the outer side is

$$I_{out} = I(1.-R_{EFL}) \qquad \text{(see 7.17)}$$

$$I_{out}/I \approx (1.-R_{EFL})^{0.66} \tag{8.9}$$

According to eq. (8.4) wall reflection therefore causes a reduction of the cyclotron radiation losses by a factor of $(1.-R_{EFL})^{0.66}$.

For 5 keV < T_M < 15 keV one has the following rough approximation: $\hat{E} = 0.35$. From this it follows that:

The dependence on the density is $\frac{\partial^2 E}{\partial F \partial t}$ prop. $n_e^{0.35}$.

The dependence on the temperature is: $\frac{\partial^2 E}{\partial F \partial t}$ prop. $T_e^{2.3}$.

The dependence on the magnetic field is $\frac{\partial^2 E}{\partial F \partial t}$ prop. $\omega_H^{2.65}$.

The intensity in the plasma torus depends on the parameters

$D,\ p_t,\ R_{EFL},\ T_M,\ \phi_A,\ A_{SPEKT}$

with

$$A_{SPEKT} = R_G/R_K$$

We have numerically computed about 20 intensities for

$D = 1200.$ $\qquad$ $\phi_A = 0$ (test point "inside")

$2 \leq T_M \leq 10$ keV $\qquad$ $\phi_A = 3.14$ (test point "outside")

$p_D = p_T = 1$

$2 \leq A_{SPEKT} \leq \infty$

The results can be given by

$$I = I_{cyl}\left[1 + \frac{20}{A_{SPEKT}\ T_M}\right] \qquad \text{for } \phi_A = 0 \qquad (8.11)$$

$$I = I_{cyl}\left[1 + \frac{7}{A_{SPEKT}\ T_M}\right] \qquad \text{for } \phi_A = 3.14$$

with about 10-20% inaccuracy.*

It is seen that the torus intensity I is about 1.5 to 3 times the cylinder value I_{cyl} -- in general, because the resonance lines in fat tori are wider than in slender tori (see fig. 16), the toroidal effect is more pronounced in fat tori. Furthermore, for low temperatures the resonance lines are narrower than for high temperatures; line-broadening due to toroidal curvature is therefore more effective at low temperatures than at high values; therefore T_M occurs in the denominator of eq. (8.11).

---

* For T_M=2 keV eq.(8.11) gives too large values about a factor 1.2-1.7

§9 Energy balance of the plasma cylinder

A plasma volume element $dV = r\, dr\, d\phi\, dz$

produces the power $dL = (P-B)\, dV$,

where P = fusion power density,

B = bremsstrahlung density,

(see Ref. /4/, §9). It is assumed that this power emerges without hindrance from the plasma surface, where it produces the intensities

$$\text{FUSION} = \frac{1}{R_K} \int_0^{R_K} P\, r\, dr \quad , \tag{9.1}$$

and

$$\text{BREMS} = \frac{1}{R_K} \int_0^{R_K} B\, r\, dr \quad . \tag{9.2}$$

In Table III this is compared with

$$\text{CYCLO} = m_e \omega_H^3\, I_{out} \quad , \tag{9.3}$$

I_{out} = intensity on "outer" side; see eq. (8.9).

Table III Energy balance of the plasma cylinder

$D_M(cm^{-3})$	P_D	FUSION	BREMS	CYCLO
$1 \cdot 10^{+13}$	2	$3{,}6 \cdot 10^5$	$3{,}6 \cdot 10^4$	$3{,}1 \cdot 10^5$
$3 \cdot 10^{+13}$	2	$3{,}2 \cdot 10^6$	$3{,}3 \cdot 10^5$	$4{,}9 \cdot 10^5$
$3 \cdot 10^{13}$	1	$5{,}9 \cdot 10^6$	$4{,}9 \cdot 10^5$	$4{,}9 \cdot 10^5$

Unit erg cm^{-2} sec^{-1}

Parameters:

H = 50 kG

R_K = 200 cm

T_M = 17 keV ; $T_i = T_e$

P_T = 2

R_{EFL} = 0,9

Everywhere in the cylinder the ion temperature is assumed to be equal to the electron temperature. For calculating FUSION we assumed a mixture of deuterium and tritium.

The 1st line represents the critical case, where gain and loss terms just cancel each other.

The 3rd line shows that a peaked temperature profile and a rounded density profile increases the fusion power* without any (appreciable) rise of the cyclotron losses (in fact, the cyclotron losses increase approx. 2 % on transition from the 2nd to the 3rd line).

---

* compared with a peaked density profile (2nd line)

§10 Calculation of the dimensionless absorption coefficient A

In accordance with ARTSIMOVICH (/3/, §46) we define the dimensionless absorption coefficient A by the equation

$$A = \frac{c\,\omega_H}{\omega_p^2}\,\alpha \quad . \tag{10.1}$$

All the quantities involved are "local", i.e. they refer to a certain point in the interior of the plasma.

We now replace

α according to eq. (10.2) by η (KIRCHHOFF),

η according to eq. (10.12)by $\tilde{I}$ and dn_e (single-particle radiation formula),

dn_e according to eq. (10.14) by a MAXWELL distribution,

and set the dielectric constant ε appearing in eq. (10.5) equal to unity (see eqs. (10.4) and (10.11)).

The integration over $dp_\perp$ (eqs. (10.12 and (10.13)) is done with the δ function occuring in eq. (10.5); the result is presented in eqs. (10.16) - (10.22). Equation (10.17) was numerically integrated both in accordance with /4/, and by expanding the BESSEL functions (see eqs. (10.27 - (10.35)). The latter method requires 10 - 20 times less computing time than /4/, §10, but is only applicable for

$$\Omega \leq 4.5 \quad \text{at} \quad T_e = 17 \text{ keV}$$

$$\Omega \leq 7.0 \quad \text{at} \quad T_e = 5 \text{ keV}$$

At very high temperatures and frequencies A can be described by an approximation formula; see eqs. (10.36) - (10.38).

==========

KIRCHHOFFS's law states that $$\eta = \alpha \frac{n_r^2 m_e \omega^2}{8\pi^3 \mu} \qquad (10.2)$$

in RAYLEIGH JEANS app.

where $$\mu = \frac{m_e c^2}{kT_e} \quad , \qquad (10.3)$$

$$\mu = \frac{511}{T_e(keV)} \quad , \qquad (10.3a)$$

and the refractive index of the plasma is $n_r = 1$. (10.4)

==========

The radiation power (erg/s) per interval of solid angle of an electron with momentum $\vec{p}$ in the magnetic field $\vec{H}$ is

$$\tilde{I} = \frac{e^2\omega^2}{2\pi\varepsilon c} \sum_{n=1}^{\infty} B_n \, \delta\left(\frac{n\omega_H}{w} - \omega \left(1 - \frac{p_{\parallel}}{w} \cos\theta\right)\right), \qquad (10.5)$$

where

$$\omega_H = \frac{eH}{m_e c} \qquad (10.6)$$

(H = magnetic field in gauss),

$\vec{p}$ = electron momentum in $m_e c$ units,

$p_{\parallel}$ = $\vec{p}$ component parallel to the magnetic field,

$$w = \sqrt{1+p^2} \quad , \qquad (10.7)$$

$$B_n w^2 = \left[\frac{w\cos\theta - p_{\parallel}}{\sin\theta}\right]^2 \cdot J_n^2 + p_{\perp}^2 J_n'^2 \quad , \tag{10.8}$$

$J_n = J_n(\text{arg})$ = BESSEL function,

$$J_n' = dJ_n/d\ \text{arg} \quad ,$$
$$\text{arg} = p_{\perp}\ \Omega\ \sin\theta \quad , \tag{10.9}$$

$$\Omega = \omega/\omega_H \quad . \tag{10.10}$$

Collective effects are ignored; every plasma electron emits as if it were in vacuum:

we therefore set

$$\varepsilon = 1 \tag{10.11}$$

Equation (10.11) and hence many conclusions drawn from it may be false:

1. for low frequencies: $\omega \leq$ hybrid frequencies, and
2. near the resonance frequencies $\omega = n\omega_H$

   in an interval of width $\Delta\omega = \omega_p^2/(n\omega_H)$.

Fortunately, owing to eqs. (5.7a), (5.12) and (5.13) A does not have to be calculated exactly at low frequencies (n = 2 or n = 3); it is sufficient to know, for example, whether the optical thickness of a resonance is large relative to unity.

Because of eq. (10.11) the emissivity is

$$\eta = \int \tilde{I}\ dn_e \quad , \tag{10.12}$$

dn_e = contribution of the momentum space element d^3p to the electron density n_e ,

$$d^3p = 2\pi p_\perp \, dp_\perp \, dp_{\shortparallel} \quad . \tag{10.13}$$

With a MAXWELL distribution of the electrons one has

$$dn_e = n_e \, c_o \exp\left(- \mu \sqrt{1+p^2} \right) d^3p \quad , \tag{10.14}$$

where

$$c_o = \frac{\mu}{4\pi K_2(\mu)} \simeq e^{\mu} \left[\frac{\mu}{2\pi \left(1+ \frac{1.28}{\mu}\right)} \right]^{3/2} \quad , \tag{10.15}$$

$K_2(\mu)$ = modified second-order HANKEL function.

This takes care of all formulae required for calculating A (eq. (10.1)). It follows that A only depends on three dimensionless variables Θ, Ω, μ:

$$A = A(\theta; \Omega; \mu) = \frac{1.2533\mu}{\Omega} \cdot \left[\frac{\mu}{1+ \frac{1.28}{\mu}} \right]^{3/2} \sum_{n=n_{min}}^{\infty} S_n \quad , \tag{10.16}$$

$$S_n = \int_{p_1}^{p_2} B_n w^2 \, e^{(1-w)\mu} dp_{\shortparallel} \quad , \tag{10.17}$$

$$n > \Omega \sin\theta \quad , \tag{10.18}$$

n_{min} = smallest integer satisfying eq. (10.18).

$$w = V + p_{\shortparallel} \cos\theta \quad , \tag{10.19}$$

$$V = n/\Omega \quad , \tag{10.20}$$

$$p_{1,2} = \sin^{-2}\theta \left[V \cos\theta \mp \sqrt{V^2 - \sin^2\theta} \right] \quad , \tag{10.21}$$

$$B_n w^2 \text{ see eq.(10.8) with } p_\perp^2 = w^2 - 1 - p_\parallel^2 \tag{10.22}$$

With the definitions

$$v_s = \frac{V^2 - \sin^2\theta}{\sin^2\theta} \quad , \tag{10.23}$$

$$a = \sqrt{v_s}\,\mu\cot\theta \quad , \tag{10.24}$$

it follows that

$$S_n = \exp\left[\mu\left(1 - \frac{V}{\sin^2\theta}\right)\right] \frac{\sqrt{v_s}}{\sin\theta} \frac{1}{a} \int_{-a}^{a} \left[v_s \left(\frac{y}{a}\right)^2 J_n^2 + \frac{(\arg J_n')^2}{(\Omega \sin\theta)^2} \right] e^{-y}\, dy \tag{10.25}$$

where

$$\arg^2 = v_s \sin^2\theta \;\; \Omega^2 \left[1 - \left(\frac{y}{a}\right)^2 \right] \quad . \tag{10.26}$$

Equation (10.25) is a good starting point for the calculation by expanding the BESSEL functions.

Let

$$h^2 = \left[\frac{\arg}{2}\right]^2 = f\, z \tag{10.27}$$

with

$$f = \frac{1}{4} v_s \sin^2\theta\, \Omega^2, \tag{10.28}$$

$$z = 1 - \left(\frac{y}{a}\right)^2 \quad . \tag{10.29}$$

It then follows that

$$J_n^2 = \left(\frac{h^n}{n!}\right)^2 \left[1 - BQ_2\, h^2 + BQ_4\, h^4 - BQ_6 h^6 + \ldots, \right. \tag{10.30}$$

$$(\arg J_n')^2 = \left(\frac{h^n}{n!}\right)^2 \left[n^2 - BA_2\, h^2 + BA_4\, h^4 - BA_6 h^6 + \ldots, \right. \tag{10.31}$$

where

$$BQ_2 = \frac{2}{n+1} \tag{10.32a}$$

$$BA_2 = BQ_2 \cdot (n+2)\,n \tag{10.32b}$$

$$BQ_4 = \frac{1}{n+1}\left[\frac{1}{n+2} + \frac{1}{n+1}\right] \tag{10.32c}$$

$$BA_4 = \frac{1}{n+1}\left[\frac{n(n+4)}{n+2} + \frac{(n+2)^2}{n+1}\right] \tag{10.32d}$$

$$BQ_6 = \frac{1}{(n+1)(n+2)}\left[\frac{1/3}{n+3} + \frac{1}{n+1}\right] \tag{10.32e}$$

$$BA_6 = \frac{1}{(n+1)(n+2)}\left[\frac{n(n+6)}{3[n+3]} + \frac{(n+2)(n+4)}{n+1}\right] \tag{10.32f}$$

Substitution in eq. (10.25) yields

$$S_n = b_{n1}\, i_{n+1} + b_{n2}\, i_{n+2} + b_{n3}\, i_{n+3} + \ldots \tag{10.33}$$

where $$b_{nk} = \frac{\hat{b}_{nk}}{[n!]^2}\,\frac{\sqrt{v_s}}{\sin\theta}\,\exp\left[a + \mu\left(1 - \frac{V}{\sin^2\theta}\right)\right], \tag{10.34}$$

$$\hat{b}_{n1} = f^n\left[\frac{n^2}{\Omega^2\sin^2\theta} + v_s\right], \tag{10.34a}$$

$$\hat{b}_{n2} = -f^{n+1}\left[\frac{BA_2}{\Omega^2\sin^2\theta} + v_s\left(\frac{1}{f} + BQ_2\right)\right], \tag{10.34b}$$

$$\hat{b}_{n3} = f^{n+2}\left[\frac{BA_4}{\Omega^2\sin^2\theta} + v_s\left(\frac{BQ_2}{f} + BQ_4\right)\right], \tag{10.34c}$$

The i_k can be integrated analytically:

$$i_{k+1} = e^{-a}\,\frac{1}{a}\int_{-a}^{a}\left[1-\left(\frac{x}{a}\right)^2\right]^k e^{-x}\,dx \tag{10.35}$$

Note the minus sign in eq. (10.34b) !

Approximation formula for high energies and frequencies

In the ranges

$$T_e > 17 \text{ keV} \quad , \qquad (10.36)$$

$$\Omega \geq 6 \quad ,$$

the resonant modes have decayed, except for a small region near $\theta \simeq 90^o$. The results obtained numerically can be represented in the ranges (10.36) by the approximation formula

$$A = a\, e^{-b\Omega^{\gamma}} \qquad (10.37) \qquad (10.37)$$

where

$$\gamma = 0.357 + 0.018 \sin^2\theta + 0.075 \ln x \qquad a)$$

$$x = 41./T_e(\text{keV}) \qquad b)$$

$$b = 6.226 \sin^{V}\theta + 0.853\, x^{W} \sin^{U}\theta \qquad c)$$

$$V = -0.287 - 0.18 \sin\theta \qquad d)$$

$$W = 0.4 + 0.33 \sin\theta \qquad e)$$

$$U = -1.58 (\sin\theta)^{0.31} \qquad f)$$

$$a = 1485.\, \sin^{E}\theta \exp\left[q\, x^{-1.1} + R\, x^{H} \right] \qquad g)$$

$$E = -4.81 + 0.55 \sin\theta \qquad h)$$

$$H = 1. + 0.3 \sin\theta \qquad i)$$

$$q = -0.81 + 0.44\sqrt{\sin\theta} \qquad k)$$

$$R = 0.51 - 0.886 \ln(\sin\theta) \qquad m)$$

The inaccuracy is

	$4 < \Omega < 8$	$8 < \Omega < 30$
$17 < T_e < 40$keV	7-200%	3%
$40 < T_e < 100$keV	4-7%	2%

Range of application:

$$0.1 < \theta \lesssim 1.57 \qquad A \gtrsim 10^{-7} \tag{10.38}$$

When the resonant modes have not yet decayed, e.g. at $\theta = 1.57$, $T_e = 17$ keV and $\Omega = 4$, eq. (10.37) is of no use. But there are also angular ranges, e.g. $\theta = 30^{\circ} - 60^{\circ}$, where eq. (10.37) can also be used for 10 keV and sometimes even down to 5 keV. Exact definition of the range of application is, however, a complicated matter; there are also, for example, ranges in which the resonant modes have decayed and eq. (10.37) is nevertheless almost of no use. Furthermore, there are also wide ranges in which eq. (10.37) is also fairly valid for very small A.

§11 Programming of torus spectra in δ approximation

We describe here a program which calculates spectra $Y(\Omega_T)$ according to §5, eq. (5.7).

For this purpose it is necessary to give the temperature (eq. (11.3)), density or plasma frequency (eq. (11.4)), magnetic field etc. as functions of s; once this has been done s is replaced by the resonance point (s) s_m and the corresponding τ_m is calculated according to eq. (5.12).

We thereby restrict ourselves to the special case $\boxed{\vartheta = 90^\circ}$ occuring almost exclusively in cyclotron spectroscopy.

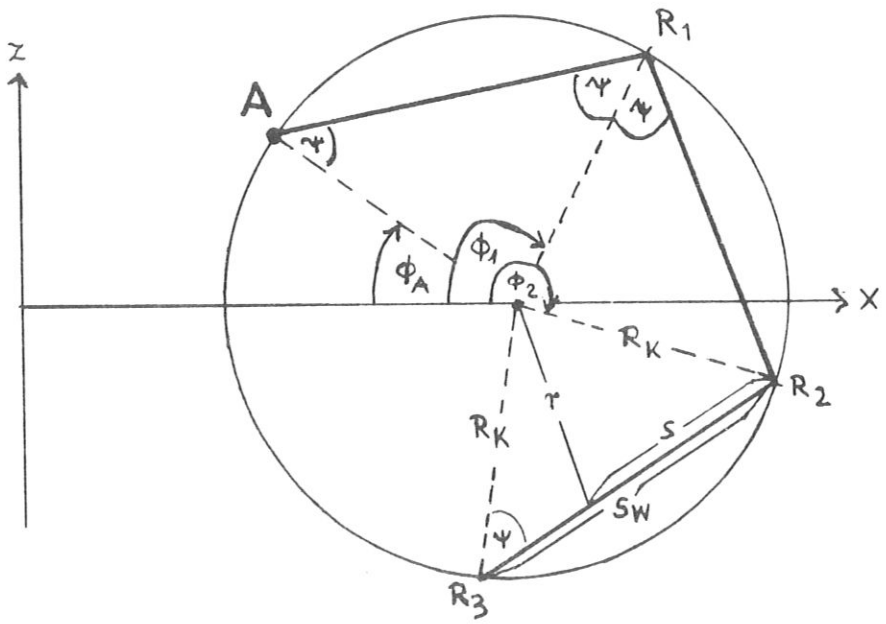

Fig. 24

The light paths (see Fig. 24; A = test point) are all located in the x-z plane; the point R_N has the coordinates

$$x_N = R_G - R_K \cos\phi_N \quad ,$$

$$y_N = 0 \quad , \qquad \text{(see 3.1)}$$

$$z_N = R_K \sin\phi_N \quad ,$$

where $$\phi_N = \phi_{N-1} + \pi - 2\psi \quad . \qquad (11.1)$$

The light path point s is at a distance r from the minor axis; in accordance with the cosine law one has

$$r^2 = R_K^2 + s^2 - 2R_K s \cos\psi$$

In addition, one takes $$q = 1 - \frac{r^2}{R_K^2} = \frac{s}{R_K}\left[-\frac{s}{R_K} + 2\cos\psi\right] \qquad (11.2)$$

According to eq. (4.1 - 2) it then follows that $T_e(s) = T_M q^{p_T}$ (11.3)

and

$$\omega_p^2(s) = \omega_M^2 q^{p_D} \qquad (11.4)$$

The light path length is given by

$$s_w = 2R_K \cos\psi. \qquad (11.5)$$

The magnetic field H depends on the distance E from the major axis; since y = 0 this distance according to eqs. (3.3) and (3.4a) is

$$E = x_N + e_x s \qquad (11.6a)$$

with $$x_N = R_G - R_K \cos\phi_N \quad , \qquad (11.6b)$$

$$e_x = \cos(\psi - \phi_N) \quad . \qquad (11.6c)$$

As long as $$H_{pol} \leq 0{,}2\ H_{tor} \qquad (11.7)$$

is satisfied, the influence of the plasma current on the cyclotron spectrum is less than 5 % and can therefore be neglected.

Although the change of direction is a first-order quantity, the influence of the plasma current on U_n according to eq. (5.13c) is of second order:

(11.7a)

$$\frac{U_n}{U_{no}} = (\sin\theta)^{2n-3} = 1 - (n - \tfrac{3}{2}) \left[\frac{H_{pol}}{H_{tor}}\right]^2 \qquad (11.7b)$$

In the case of oblique light paths with $\vartheta \neq 90^o$ the influence of the plasma current on U_n is of first order!

We now discuss SUBROUTINE YROUT:

YROUT calculates for given Ω_T = OT and ϕ_N = PN the spectral function Y according to the formulae (11.2 - 6), (5.9e), (5.11), (5.12), (5.8a) (5.14a) and (5.7). Equation (5.8a) assumes that T_e is known at the point S_n, but it still has to be calculated; the use of eq. (5.8a) thus calls for an iteration method (see ISN 0016 - 0028).

We now discuss the main program:

The mesh points Ω_T = OM(JO) at which the spectrum $Y(\Omega_T)$ = YO(JO) is to be calculated is entered in ISN 0004.

All other parameters are entered in ISN 0005:

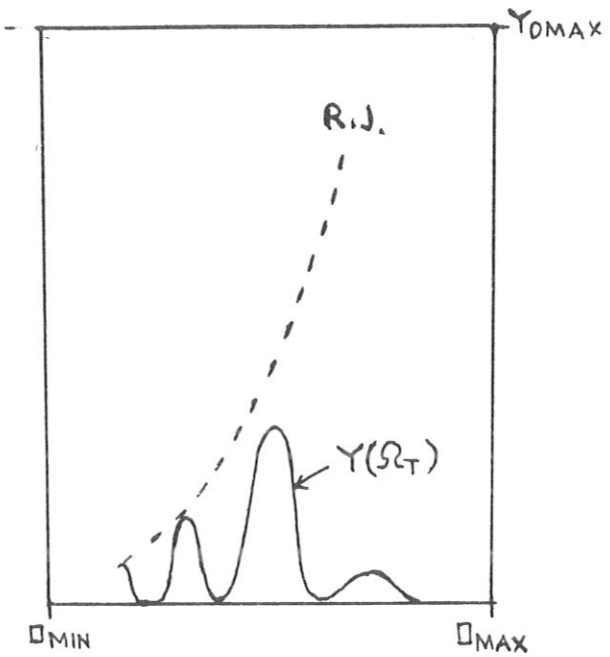

Fig. 25

OMIN, OMAX and YOMAX are the coordinates of the frame corner points of the drawing; for example one has in fig. 20:

OMIN = 2.6

OMAX = 3.0

YOMAX= 35.

Figure 20 was not produced with this program, but this has no bearing in this context.

NLI and NRE limit the Ω_T interval, on the left and right respectively, in which the spectrum is to be calculated (see ISN 0017).

NMAX is the number of reflected light paths which has to be taken into account; in Fig. 22 and 26b one has NMAX = 2.

Note: in the case of Fig. 26b NMAX is limited to 2 because there is an observation port at the test point, which does not reflect any light.

PA = ϕ_A, PS = ψ and the rest of the parameters are defined by the corresponding equations; TH = ϑ = 1.57.

The following remarks on the loop ISN 0017-29 should be noted: The IF statement 0023 is necessary because the computer cannot compute 0^M.

ISN 0025 corresponds to eq. (11.1);

ISN 0026 corresponds to the exponent in eq. (5.7) and (7.2)

ISN 0028 corresponds to eq. (7.12).

```
C TORUS SPEKTREN  APPROXIMATION DURCH DELTA-FUNKTIONEN
0001        REAL*4       MY
0002        DIMENSION    OM(72) , X(5) , Y(5) , YO(72)
0003        COMMON   COSPS, FO, OT, PD,PN,PS,PT, RG,RK, SW, TAUC,TM, YR,YY
0004        READ 118,    ( OM(JO) , JO=1,72)
0005       10 READ  316,    NLI, NRE, NMAX, DM, HT, OMIN, OMAX, PA, PD, PS, PT
          1                                , REFL, RG, RK, TH, TM, YOMAX
0006            RG = RG * 100.
0007            RK = RK * 100.
0008         COSPS = COS(PS)
0009            SW = 2.* RK* COSPS
0010         COSPA = COS(PA)
0011            FO = 60.36 * DM / HT
0012         PRINT 98
0013         PRINT 91
0014         PRINT 317,    NLI, NRE, NMAX, DM, HT, OMIN, OMAX, PA, PD, PS, PT
            1                                , REFL, RG, RK, TH, TM, YOMAX
0015         PRINT 96
0016         PRINT 93
0017         DO 8       JO=NLI,NRE
0018            OT = OM(JO)
0019            PN = PA
0020         CALL YROUT
0021            SY = YY
0022           TAU = 0.
0023         IF ( REFL. LE. 0.1)       GO TO 8
0024         DO 6       M=1,NMAX
0025            PN = PN + 3.1416 - 2.*PS
0026           TAU = TAU + TAUC
0027         CALL YROUT
0028        6      SY = SY + REFL**M * EXP(-TAU) * YY
0029        8 YO(JO) = - SY
0030           YMIN = - YOMAX
0031           YMAX = 0.
0032           Y(1) = YMIN
0033           X(1) = OMIN
0034           Y(2) = YMIN
0035           X(2) = OMAX
0036           Y(3) = YMAX
0037           X(3) = OMAX
0038           Y(4) = YMAX
0039           X(4) = OMIN
0040           Y(5) = YMIN
0041           X(5) = OMIN
0042         CALL FRAME ( YMIN , OMIN , YMAX , OMAX )
0043         CALL PLOTL ( Y , X , 5 )
0044         CALL PLOTL ( YO , OM , NRE )
0045         DO 9       J=NLI,NRE
0046         PRINT 112,    OM(J), YO(J)
0047        9  YO(J) =-TM* OM(J)**2                    ← Rayl. Jeans Parabola
0048         CALL PLOTLS( YO , OM , NRE )
0049         GO TO 10
0050        91 FORMAT(116H    NLI    NRE  NMAX     DM     HT  OMIN  OMAX      PA      P
          1D       PS     PT   REFL     RG     RK       TH          TM     YOMAX)
0051        92 FORMAT(/29H         EX          XA          FO)
0052        93 FORMAT(122H         OT           Y          YR      T(N=2        N=3
          1 N=4)    TAU(N=2        N=3        N=4)      S(N=2        N=3          N=4
          2))
0053        96 FORMAT (1H )
0054        98 FORMAT (1H1)
0055       112 FORMAT ( 3F10.2 , 6F10.3 , 3F10.1 )
0056       118 FORMAT ( 18F4.1)
0057       316 FORMAT ( 3I4 , 15F4.1)
0058       317 FORMAT ( 3I6 , 4F6.1 , F8.3 , F6.1 , F8.3 , F6.1 , F7.2 , 2F7.1
          1      , F8.3 , 2F8.1 )
0059            END
```

```
0001                SUBROUTINE YROUT
0002                DIMENSION   S(5) ,T(5) ,TAU(5)
0003                COMMON   COSPS, FO, OT, PD,PN,PS,PT, RG,RK, SW, TAUC,TM, YR,YY
0004                 COSPN = COS(PN)
0005                    YR = 0.
0006                  TAUC = 0.
0007              1     EX = COS(PS-PN)
0008                   AEX = ABS ( EX )
0009                    XA = RG - RK* COSPN
0010                DO 5       L=1,5
0011                IF ( EX. LT. 0.)       GO TO 2
0012                     N = L
0013                GO TO 3
0014              2      N = 6 - L
0015              3     MY = 1000.
0016                DO 33       IT=1,2
0017                ORES = N / (0.8*(1.+N)/MY   +  1.)
0018                    SN = ( RG * ORES/OT - XA) / EX
0019                  S(N) = 0.
0020                  T(N) = 0.
0021                TAU(N) = 0.
0022                    TE = 0.
0023                IF ( SN. GE. SW. OR. SN. LE. 0.)          GO TO 4
0024                  S(N) = SN
0025                    SR = SN/RK
0026                     Q = SR* (2.*COSPS - SR)
0027                    TE = TM *  Q**PT
0028             33     MY = 511. / TE
0029                    UN = (0.01*TE)**(N-1) * (134./(N-0.9) - 7. - TE)**3
                  1          / (1.6E9 *4050.**(1-N) + 2.55 * 8.3**(8-N))
0030                     E = XA + EX *SN
0031                  TAUN = FO* UN* E*  Q**PD / (OT*AEX)
0032                TAU(N) = TAUN
0033              4   T(N) = TE * EXP(-TAUC) * (1.- EXP(-TAU(N)))
0034                  TAUC = TAUC + TAU(N)
0035              5     YR = YR + T(N)
0036              7     YY = YR * OT**2
0037              8 PRINT 112,   OT,YY, YR, (T(N),N=2,4) ,(TAU(N),N=2,4) ,(S(N),N=2,4)
0038              9 RETURN
0039             112 FORMAT ( 3F10.2 , 6F10.3 , 3F10.1 )
0040                END
```

NLI	NRE	NMAX	DM	HT	OMIN	OMAX	PA	PD	PS	PT	REFL	RG	RK	TH	TM	YOMAX
1	60	1	10.0	31.0	0.0	8.0	3.140	0.0	0.0	2.0	0.0	290.0	130.0	1.570	3.0	90.0

DT	Y	YR	T(N=2	N=3	N=4)	TAU(N=2	N=3	N=4)	S(N=2	N=3	N=4)
1.00	3.00	3.00	0.0	0.0	0.0	0.0	0.0	0.0	0.0	0.0	0.0
1.10	3.29	2.72	0.0	0.0	0.0	0.0	0.0	0.0	0.0	0.0	0.0
1.20	3.14	2.18	0.0	0.0	0.0	0.0	0.0	0.0	0.0	0.0	0.0
1.30	2.67	1.58	0.0	0.0	0.0	0.0	0.0	0.0	5.8	0.0	0.0
1.40	0.44	0.23	0.018	0.0	0.0	1.605	0.0	0.0	34.5	0.0	0.0
1.50	1.43	0.63	0.635	0.0	0.0	38.491	0.0	0.0	60.0	0.0	0.0
1.60	3.87	1.51	1.511	0.0	0.0	78.387	0.0	0.0	71.5	0.0	0.0
1.65	5.19	1.91	1.908	0.0	0.0	91.914	0.0	0.0	82.3	0.0	0.0
1.70	6.49	2.25	2.246	0.0	0.0	100.856	0.0	0.0	92.3	0.0	0.0
1.75	7.71	2.52	2.517	0.0	0.0	105.785	0.0	0.0	101.8	0.0	0.0
1.80	8.82	2.72	2.723	0.0	0.0	107.470	0.0	0.0	110.6	0.0	0.0
1.85	9.81	2.87	2.868	0.0	0.0	106.635	0.0	0.0	118.9	0.0	0.0
1.90	10.67	2.96	2.956	0.0	0.0	103.918	0.0	0.0	126.7	0.0	0.0
1.95	11.39	3.00	2.996	0.0	0.0	99.854	0.0	0.0	134.0	0.0	0.0
2.00	11.98	2.99	2.994	0.0	0.0	94.861	0.0	0.0	141.0	0.0	0.0
2.05	12.43	2.96	2.957	0.0	0.0	89.272	0.0	0.0	147.6	5.8	0.0
2.10	12.75	2.89	2.890	0.000	0.0	83.344	0.000	0.0	153.8	15.9	0.0
2.15	12.76	2.76	2.757	0.002	0.0	77.274	0.016	0.0	159.7	25.5	0.0
2.20	12.10	2.50	2.468	0.032	0.0	71.206	0.088	0.0	165.4	34.9	0.0
2.25	10.90	2.15	2.011	0.141	0.0	65.233	0.246	0.0	170.8	43.9	0.0
2.30	9.83	1.86	1.490	0.368	0.0	59.445	0.493	0.0	175.9	52.5	0.0
2.35	9.48	1.72	1.024	0.692	0.0	53.896	0.809	0.0	180.8	60.8	0.0
2.40	9.98	1.73	0.674	1.059	0.0	48.628	1.162	0.0	185.5	68.7	0.0
2.45	11.14	1.86	0.439	1.417	0.0	43.654	1.523	0.0	190.1	76.2	0.0
2.50	12.68	2.03	0.290	1.739	0.0	38.993	1.857	0.0	194.4	83.4	0.0
2.55	14.39	2.21	0.198	2.015	0.0	34.648	2.153	0.0	198.6	90.3	0.0
2.60	16.11	2.38	0.142	2.241	0.0	30.621	2.396	0.0	202.6	96.8	0.0
2.65	17.77	2.53	0.107	2.424	0.0	26.914	2.583	0.0	206.5	103.1	0.0
2.70	19.33	2.65	0.085	2.566	0.0	23.508	2.713	0.0	210.2	109.0	0.0
2.75	20.73	2.74	0.071	2.671	0.0	20.401	2.787	0.0	213.9	114.8	5.8
2.80	21.99	2.80	0.061	2.743	0.000	17.579	2.814	0.000	217.4	120.2	13.4
2.85	23.07	2.84	0.055	2.785	0.000	15.026	2.798	0.000	220.7	125.5	20.9
2.90	23.98	2.85	0.051	2.800	0.000	12.731	2.746	0.000	224.0	130.5	28.2
2.95	24.68	2.84	0.047	2.789	0.000	10.680	2.664	0.001	227.2	135.4	35.3
3.00	25.18	2.80	0.045	2.751	0.002	8.857	2.561	0.003	230.3	140.0	42.2
3.05	25.46	2.74	0.043	2.689	0.005	7.249	2.439	0.006	233.3	144.5	48.9
3.10	25.53	2.66	0.040	2.604	0.013	5.842	2.305	0.012	236.2	148.8	55.4
3.15	25.40	2.56	0.037	2.496	0.026	4.621	2.163	0.019	239.0	153.0	61.8
3.20	25.08	2.45	0.033	2.371	0.045	3.574	2.017	0.029	241.7	157.0	67.7
3.25	24.62	2.33	0.028	2.232	0.070	2.688	1.870	0.040	244.4	160.8	73.5
3.30	24.03	2.21	0.022	2.083	0.101	1.950	1.723	0.052	246.9	164.6	79.2
3.40	22.54	1.95	0.009	1.770	0.170	0.871	1.440	0.076	249.5	168.2	84.6
3.50	20.82	1.70	0.001	1.459	0.239	0.250	1.180	0.097	254.3	175.1	94.8
3.60	18.93	1.46	0.000	1.166	0.295	0.009	0.949	0.112	258.9	181.6	104.4
3.70	16.88	1.23	0.0	0.903	0.330	0.0	0.750	0.121	0.0	187.8	113.3
3.80	14.71	1.02	0.0	0.676	0.342	0.0	0.581	0.122	0.0	193.6	121.6
3.90	12.54	0.82	0.0	0.488	0.336	0.0	0.441	0.119	0.0	199.1	129.4
4.00	10.47	0.65	0.0	0.339	0.314	0.0	0.328	0.111	0.0	204.4	136.7
4.10	8.60	0.51	0.0	0.225	0.282	0.0	0.238	0.101	0.0	209.4	143.5
4.20	6.97	0.40	0.0	0.143	0.245	0.0	0.169	0.090	0.0	214.2	150.0
4.30	5.62	0.30	0.0	0.086	0.206	0.0	0.116	0.078	0.0	218.8	156.1
4.40	4.53	0.23	0.0	0.049	0.169	0.0	0.077	0.066	0.0	223.2	161.9
4.50	3.66	0.18	0.0	0.026	0.136	0.0	0.049	0.056	0.0	227.4	167.4
4.60	2.97	0.14	0.0	0.013	0.106	0.0	0.030	0.046	0.0	231.4	172.7
4.70	2.42	0.11	0.0	0.006	0.081	0.0	0.017	0.037	0.0	235.3	177.7
4.80	1.98	0.09	0.0	0.002	0.061	0.0	0.009	0.029	0.0	239.0	182.4
4.90	1.61	0.07	0.0	0.001	0.044	0.0	0.004	0.023	0.0	242.6	187.0
5.00	1.31	0.05	0.0	0.000	0.032	0.0	0.002	0.018	0.0	246.1	191.4
5.10	1.06	0.04	0.0	0.000	0.022	0.0	0.001	0.014	0.0	249.5	195.6
5.20	0.85	0.03	0.0	0.000	0.015	0.0	0.000	0.010	0.0	252.7	199.7

↑ see fig. 13

↑ ↑ see fig. 12

§12 Application to TFR measurements

In Ref. /5/ COSTLEY and the TFR group present measurements on the TFR tokamak and theoretical predictions for 2 light paths a) and b) (see Fig. 26 of our report) and 2 sets of parameters A) and B) (see Figs. 27 and 31 of our report). We have used the program described in §11 for these sets of parameters; the results are shown in Figs. 27-31. To calculate the peaks in Fig. 28, we used another program based on s mesh point integrating.

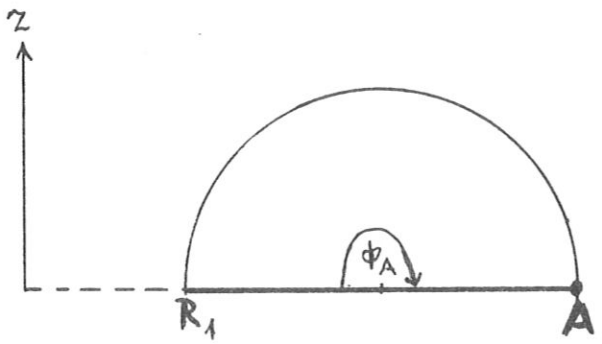

Fig. 26

The light paths used in Ref. /5/

a) $\phi_A = 180^o$

$\psi = 0$

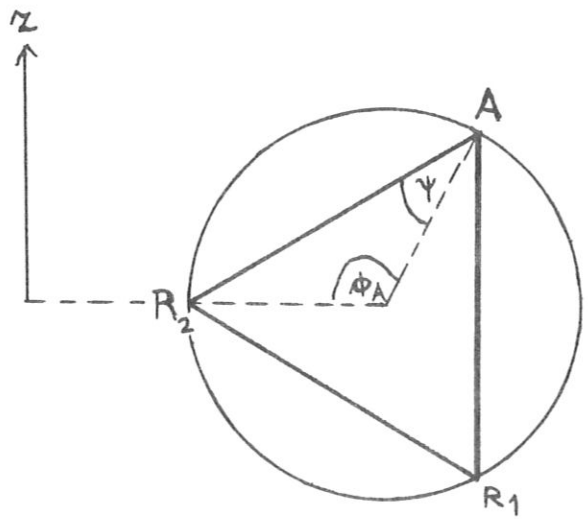

b) $\phi_A = 120^o$

$\psi = 30^o$

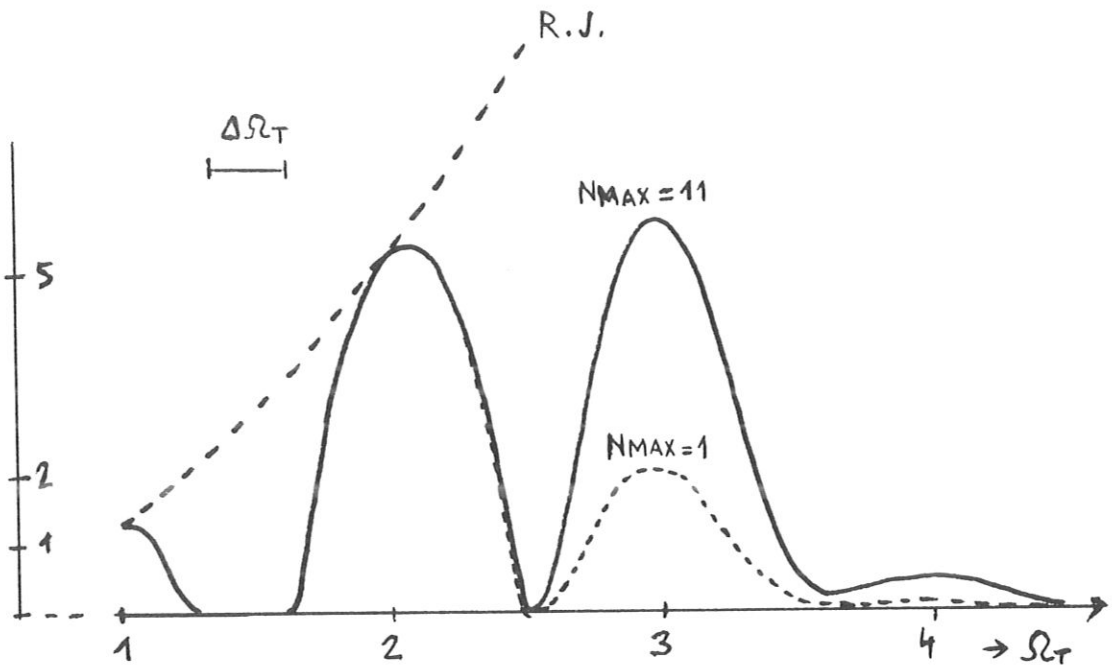

Fig. 27

Spectra Y versus Ω_T for various values of NMAX.

Parameters (set A):

$n_{eo} = D_M = 5 \times 10^{13}$ cm^{-3}

$H_T = 26$ kG

$P_D = P_T = 1$ (parabola profile)

$R_{EFL} = 0.9$

$T_{eo} = T_M = 1.3$ keV

$R_G = 98.$ cm

$R_K = 20.$ cm

Light path a)

$\phi_A = 3.14$

$\psi = 0$

Experimental resolution:

$\Delta\Omega_T \simeq 0.3$

Figure 27 corresponds to FIG. 1 in Ref. /5/ for radial emission. The experimental value for the intensity ratio $Y(\Omega_T = 3) / Y(\Omega_T = 2)$ is reproduced fairly well by our curve with NMAX = 1. This is physically reasonable because according to Fig. 26a the light should only be reflected once from R_1 and then vanish in the observation port A.

The predicted curve from Ref. /5/, FIG. 1, agress roughly with our NMAX = 11 curve.

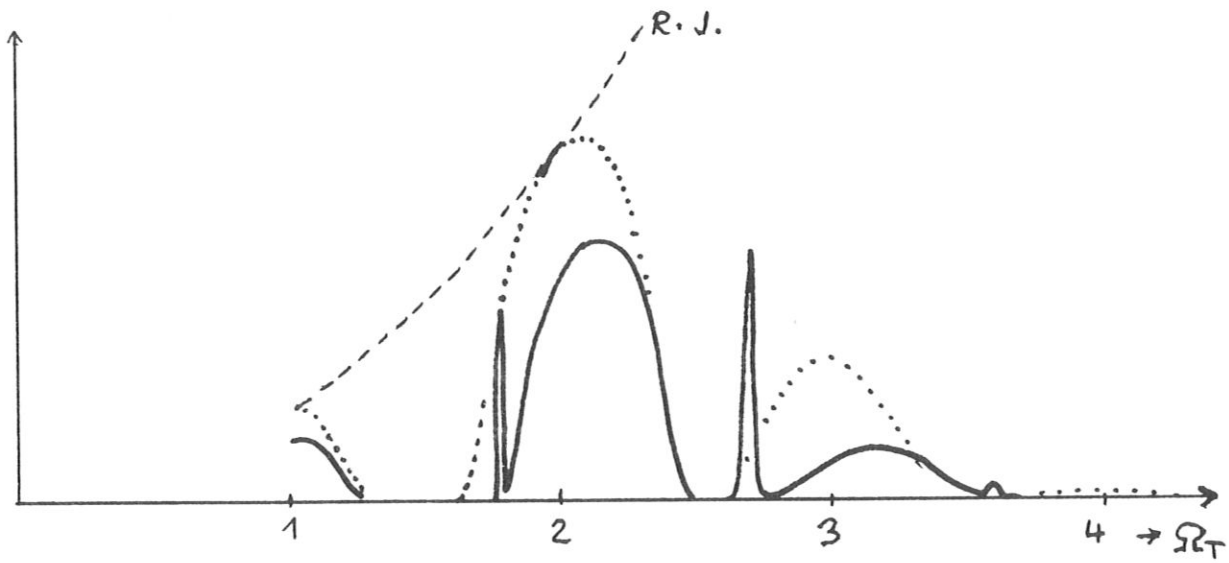

Fig. 28

a) Repetition of Fig. 27 for NMAX = 1 (dotted)

b) Spectrum for set A) of parameters and light path b) ($\phi_A = 120^o$, $\psi = 30^o$) for NMAX = 2, i.e. <u>one</u> reflection each from R_1 <u>and</u> R_2

The peaks at $\Omega_T = 1.8, 2.7, 3.6$ belong to light path R_1A in Fig. 26b and were calculated with another program which performs the s integration

in eq. (2.17) numerically by means of appropriate s mesh points. The program described in §11 does not yield any peaks owing to condition (5.19), which is not satisfied on light path R_1A owing to $ds/d\Omega \to \infty$. From eqs. (2.18), (4.11), (5.5) and (5.8) it follows that peaks are to be expected for frequencies $\Omega_T \approx n \frac{R_G}{E}$, where E denotes the distance of the light path R_1A from the major axis.

The smooth part of curve b) comes from the reflected light paths AR_2 and R_2R_1 (Fig. 26b) and is shifted to higher frequencies relative to a) because the magnetic field on AR_2R_1 is higher on the average than on a).

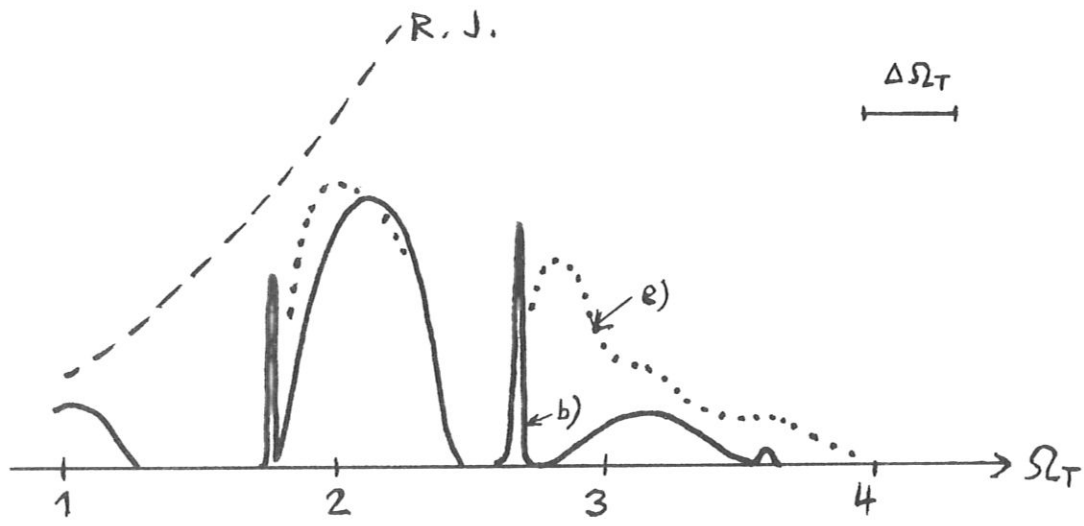

Fig. 29 Comparison of theory and experiment

b) Repetition of Fig. 28b,

e) Experimental curve (dotted), FIG. 1b in Ref. /5/.

A comparison of theory b) and experiment e) shows that the ratio I_3/I_2 of relative intensities is roughly twice as large in the experimental curve e) as in the theoretical curve b). Possible causes such as higher electron temperature, NMAX > 2, etc. are discussed later in connection with set B) of parameters. Curve e) has its maximum at $\Omega_T \simeq 2.85$ and is thus clearly shifted to lower frequencies relative to curve a) for radial emission. In addition, curve e) has a shoulder at $\Omega_T \simeq 3.2$. This might be interpreted by assuming that the peak is strongly broadened at $\Omega_T = 2.7$ as a result of the experimental conditions but loses very little amplitude in the process. Perhaps there are much more than two reflections, so that NMAX >> 2, which could explain the high intensity observed in the experiment at $\Omega_T \gtrsim 2.8$.

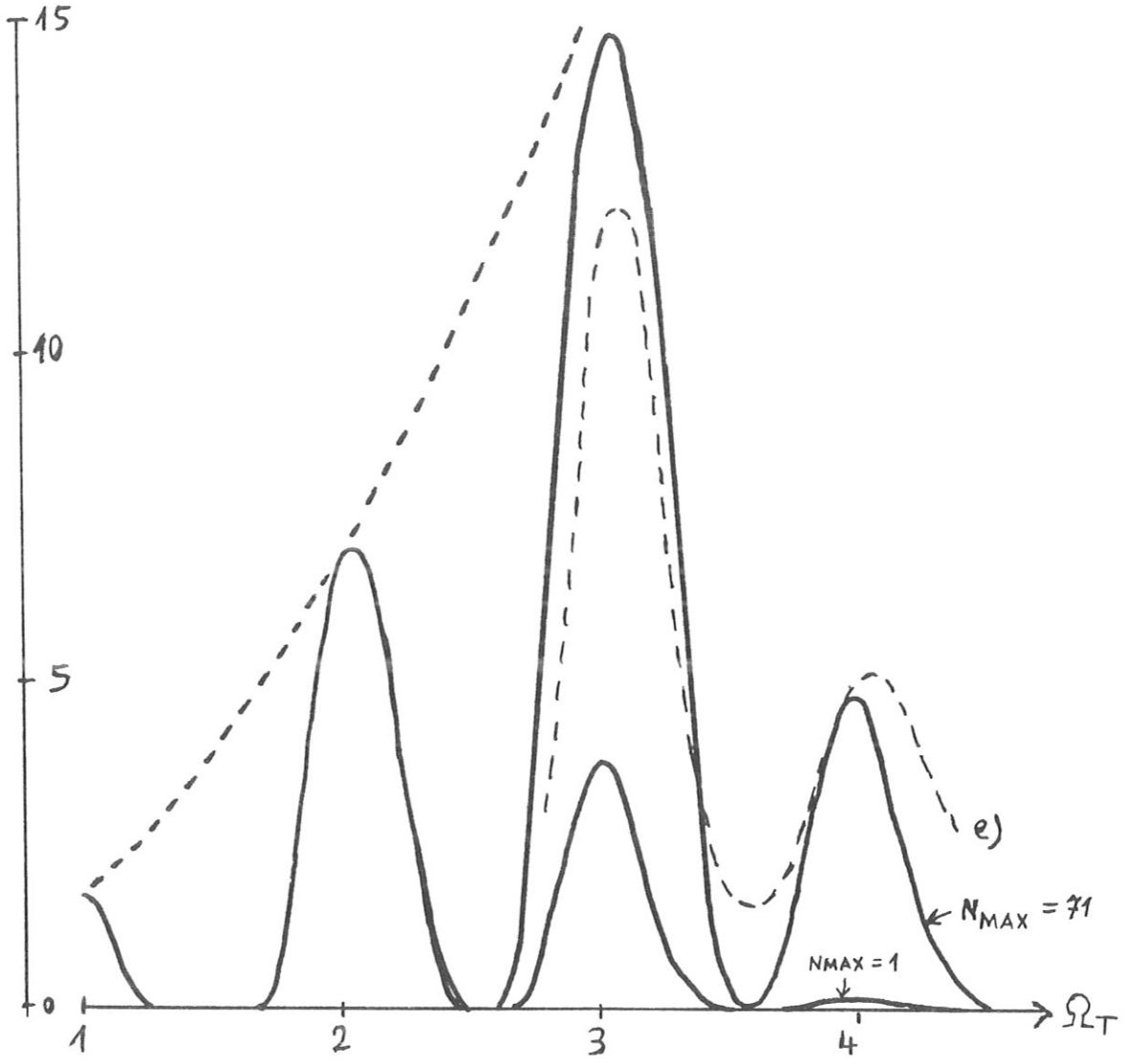

Fig. 30

Spectra Y versus Ω_T: comparison of theory and experiment e)

Set B) of parameters :

$n_{eo} = D_M = 5 \cdot 10^{13}$ cm^{-3}

$B_o = H_T = 39$ kG

$R_{EFL} = 0.99$

$p_D = 1$

$p_T = 3$(peaked temperature profile)

$R_G = 98$ cm

$R_K = 20$ cm

$T_M = 1.8$ keV

Light path a):

$\phi_A = 180^o$

$\psi = 0$

NMAX = 1 and 71

To fig. 30:

The curves for NMAX = 1 and NMAX =71 (solid) were drawn according to §11, while curve e) (dashed) is taken from Ref. /5/, FIG. 2. The line width depends on the temperature profile number p_T; The scale and p_T are chosen such that the curves coincide in the region of $\Omega_T = 2$. The lines in FIG. 2 from Ref. /5/ are more slender than those from FIG. 1; this is taken into account by setting

$p_T = 1$ in Figs. 27 and 28, but

$p_T = 3$ in Fig. 30.

Of the two theoretical curves (§11) only that with NMAX = 71 agrees to a certain extent with the experiment (curve e). NMAX = 71 means that the light generated in the plasma is reflected back and forth between the walls 71 times before disappearing in the observation port A (Fig. 26a). This is possible if one has for the experimental setting inaccuracies

$$\Delta\phi_A, \ \Delta\psi, \ \Delta\vartheta \ \geq \pm \frac{U}{8R_K} \ , \tag{12.4}$$

where U is the diameter of the observation port.

Figure 31 shows how the factor 8 arises:

The test point A is located at the centre of the observation port. Whenever

$$AA' = 4R_K\Delta\psi \geq \pm \frac{U}{2} \tag{12.4a}$$

is satisfied, the receiver in A can record light from light path $N \geq 2$ since this light is reflected at A', not absorbed.

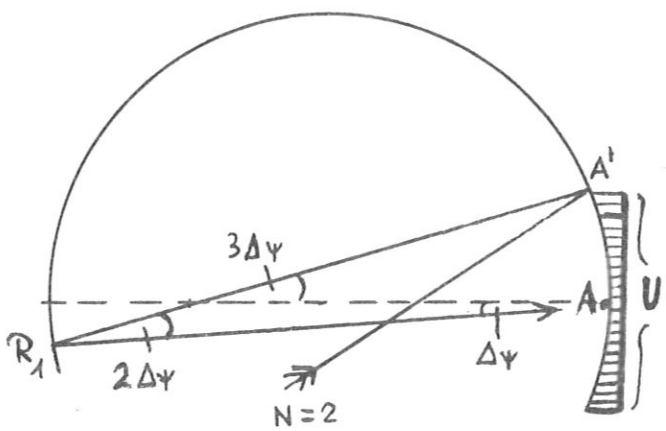

Fig. 31

There are no other possibilities of producing curves of type 30e) by means of the program from §11 for, if NMAX = 1 is retained, electrons with $T_e \gg 1.8$ keV have to be postulated to account for the n = 4 emission. At $T_e \approx 5$ keV the n = 4 maximum is, however, so strongly shifted to the left that an interpretation of this kind does not seem possible. (see fig 32)

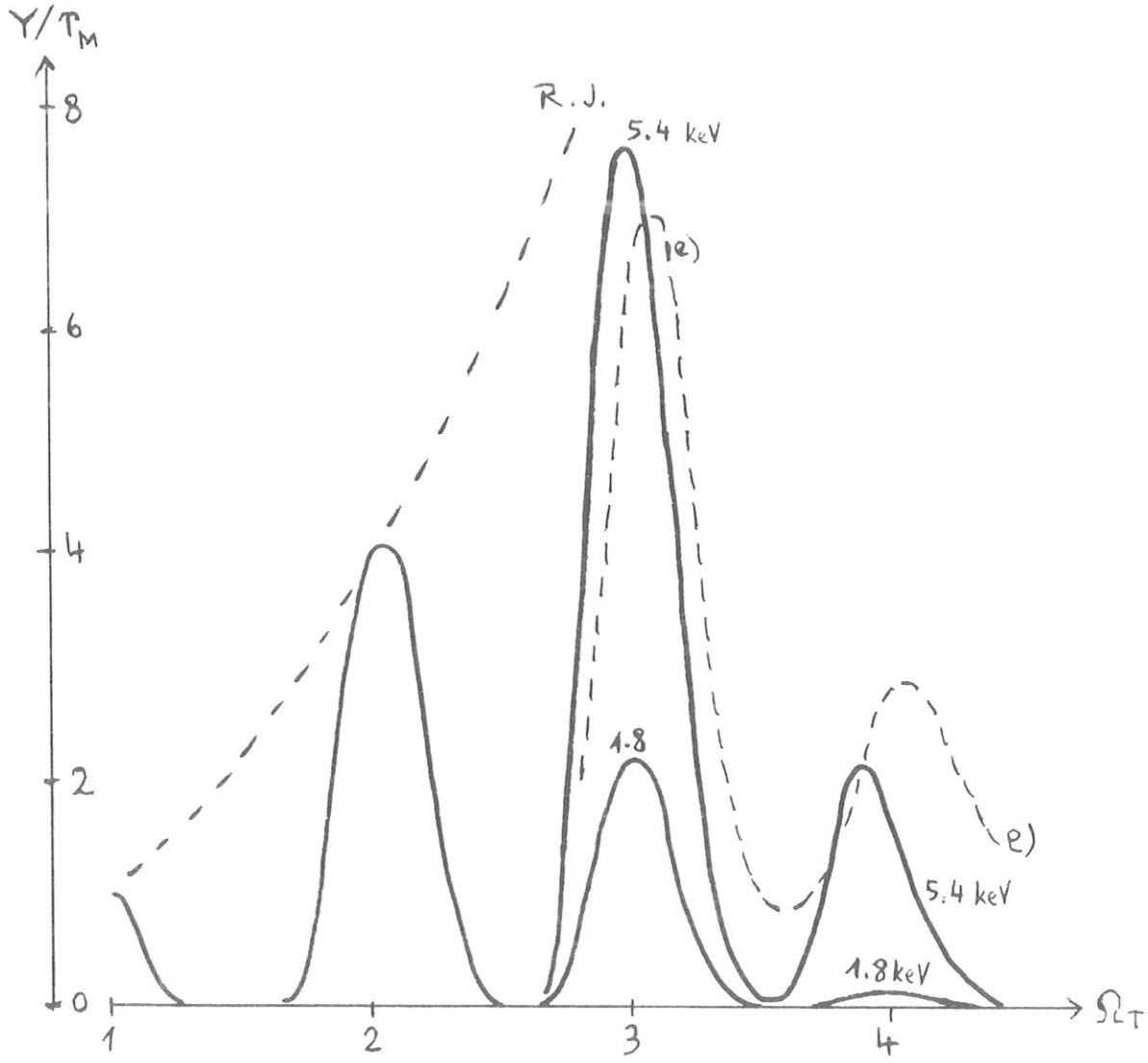

Fig. 32

Repetition of Fig. 30 and Comparison with the spectrum for T_M = 5.4 keV.

Symbol Table

1) Latin Symbols

$A(\theta;\Omega;\mu)$	(2.19); (10.1); (10.16)	dimensionless absorption coefficient
A_M	(6.2)	A at the cylinder axis
a	(5.9c)	
b	(5.9d)	
c	(2.14a)	velocity of light
$\vec{c} = \vec{e}_N$	(7.15)	direction of light path nr. N
$\vec{D}$	(7.15)	
D	(6.4d)	dimensionless cylinder radius
D_M	(4.1)	plasma density at the axis
$\frac{\partial^2 E}{\partial S \partial t}$	(2.7)	intensity of cyclotron radiation
dV	(2.6)	volume element
$d\tilde{\Omega}$	(2.5)	solid angle interval
$d\Omega_T$	(2.16)	frequency interval
e	(10.6)	elementary charge
$\vec{e} = \vec{e}_{N-1}$	(7.15)	direction of light path nr. N-1
E	(3.4a)	distance from major torus axis
$\hat{E}$	(8.2)	
$E_N(s)$	(7.3)	distance from major torus axis
e_{xN}	(7.3)	x component of $\vec{e}_N$
$\vec{f}$	(7.14)	direction of plasma surface normal
g	(7.14a)	
H, $\vec{H}$	(3.5)	magnetic field
H_{pol}	(4.12)	poloidal component

H_{tor}	(4.11)	toroidal component
H_T	(4.11)	toroidal component at the axis
I	(2.15)	dimensionless intensity
I_o	(6.7)	prop. spectral function
I_{out}	(8.9)	intensity outside
I_p	(4.12)	plasma current
I_{cyl}	(8.1)	
J_n	(10.8)	BESSEL function
k	(2.14a)	BOLTZMANN constant
m	(§5)	counts the resonances according to their distance from the test point
m_e	(2.14a)	electron mass
M	(6.4a)	profile number
n	(§5)	number of harmonic
N	(§7)	light path number
N_{MAX}	(§11)	number of reflection light pathes
n_e	(4.1)	plasma electron density
P	(6.4b)	profile number
$\hat{P}$	(8.5)	profile factor
P_A	(6.2)	profile number of absorption coefficient
P_D	(4.1)	profile number of plasma electron density
P_T	(4.2)	profile number of plasma electron temperature
$\vec{Q}$	(7.15d)	
R	(8.3)	reflectivity factor
r	(3.4b)	distance from minor torus axis

$\hat{r}$	(4.3)	
R_{EFL}	(7.1)	wall reflectivity
R_G	(3.1)	major torus radius
R_K	(3.1)	minor torus radius
$r_N(s)$	(7.4)	distance from minor torus axis
s	(2.2)	distance from the test point, measured on the light path
S	(8.4)	
s_m	(5.1)	
S_n	(5.8)	
s_w	(2.7)	light path length
s_{wN}	(7.11)	length of light path nr. N
T_e	(4.2)	electron temperature
$T_{eN}(s)$	(7.5)	
T_M	(4.2)	electron temperature at the axis
T_n	(5.12)	optical depth of the n^{th} harmonic
U_n; U_{no}	(5.13)	
Y	(2.17)	Spectral function
Y_r	(5.6), (6.5a)	
x, y, z	(3.3)	
x_A, y_A, z_A	(3.1)	coordinates of the test point
x_N, y_N, z_N	(7.3)	coordinates of reflection points

2) Greek symbols

$\alpha(s)$	(2.19)	absorption coefficient
$\alpha_N(s)$	(7.7)	
η	(2.14)	emissivity
ϑ	(2.1)	
$\theta(s)$	(2.3)	angle between the magnetic field and light path
$\tilde{\vartheta}$	(3.4c)	toroidal coordinate
μ	(10.3)	
$\tau(s)$	(2.8)	optical depth
τ_c	(7.16)	
τ_{NC}	(7.11)	
τ_D	(6.4c)	
τ_N	(7.10)	
τ_P	(6.7)	
$\tilde{\phi}$	(3.4e)	toroidal coordinate
Φ_A	(3.1)	test point coordinate
ω	(2.18)	frequency (sec^{-1})
ω_H	(10.6)	gyration frequency
ω_{HN}	(7.9)	
ω_M	(6.4e)	plasma frequency at the axis
ω_p	(6.4e)	plasma frequency
ω_{pN}	(7.8)	
ω_T	(2.18)	

Ω (10.10) ($\Omega = \omega/\omega_H$)

Ω_T (2.18) ($\Omega_T = \omega/\omega_T$) dimensionless frequency

Acknowledgement

The author wishes to thank M. Hellberg and D. Düchs for helpful discussions.

References

/1/ R. CANO, Course Plasma Diagnost. Data Acquis. Syst. (1975), p. 102

/2/ F. ENGELMANN, M. CURATOLO, Nucl. Fusion 13 (1973), p. 497

/3/ L. ARTSIMOVICH, Controlled thermonuclear reactions
Oliver & Boyd (1964)

/4/ F. POHL, J. HENNING, D. DÜCHS
IPP 6/132 Nov. 1975

/5/ A.E. COSTLEY and TFR Group
Phys.Rev.Letters, Volume 38, Number 25, June 1977, p. 1477

/6/ A.E. COSTLEY et al.
Phys.Rev.Letters, Volume 33, 1974, p.758

/7/ C.M. CELATA , D.A. BOYD
Department of Physics and Astronomy, University of Maryland
Technical Report Number 77-008 Preprint #607P030
Synchrotron Radiation as a Diagnostic Tool for Tokamak Plasmas